OVERTOPPING LAYER THICKNESS AND OVERTOPPING FLOW VELOCITY ON MOUND BREAKWATERS

PATRICIA MARES-NASARRE*, GLORIA ARGENTE, M. ESTHER GÓMEZ-MARTÍN, JOSEP R. MEDINA

[a] *Lab. Ports and Coasts, Institute of Transport and Territory, Universitat Politècnica de València, Camino de Vera s/n, 460022 Valencia, Spain*

*patmana@cam.upv.es**, *gloargar@cam.upv.es, mgomar00@upv.es, jrmedina@upv.es*

ABSTRACT

Mound breakwater design is evolving owing to rising sea levels caused by climate change and social concern regarding the visual impact of coastal structures. The crest freeboard of coastal structures tends to decrease while overtopping hazard increases over time. Pedestrian safety when facing overtopping events on coastal structures has been assessed considering the overtopping layer thickness (OLT) and overtopping flow velocity (OFV). This paper proposes a new method to estimate the OLT and OFV on mound breakwater crest during extreme overtopping events, based on 123 2D small-scale physical tests of conventional low-crested mound breakwaters with a single-layer Cubipod® and double-layer rock and cube armors. The new method to estimate OLT exceeded by 2% of incoming waves is based on formulas given in literature for dikes, but adapted and calibrated for mound breakwaters. The formula to estimate the OFV exceeded by 2% of incoming waves is based on the correlation between the statistics of the OLT and OFV, considering an empirical coefficient calibrated for each type of armor layer. Exponential and Rayleigh distribution functions are proposed for estimating the OLT and OFV with exceedance probabilities under 2%. Although the statistics of OLT and OFV depend on similar variables, contrary to intuition, specific OLT and OFV corresponding to the same overtopping event appear to be independent.

Keywords: mound breakwater, overtopping, overtopping layer thickness, overtopping flow velocity, Cubipod®, low-crested structures

1. Introduction

Crest elevation is a key factor in the design of mound breakwaters, as it affects the economic cost of the structure and its visual impact. The mean wave overtopping rate is typically considered for this end [1]; however, maximum individual volumes associated with the largest overtopping events are not directly characterized by the mean overtopping discharge. These extreme overtopping events are critical for the hydraulic stability of the breakwater crest and rear side [2], as well as for pedestrian safety when standing on the structure.

Increasing social pressure to diminish the visual impact of coastal structures, and the sea level rise and stronger wave conditions caused by climate change [3] result in a reduction of the design dimensionless crest freeboard. Thus, overtopping rates and hazards to humans are expected to increase over time.

The overtopping layer thickness (OLT) and overtopping flow velocity (OFV) have been considered to estimate the overtopping hazard for humans (see [4] and [5]). Fig. 1 shows the thresholds for the OLT, h_c (m), and OFV, u_c (m/s), on the breakwater crests proposed by Bae et al. [4] for pedestrian safety, as well as the experimental results of pedestrian failure from different authors [6, 7, 8 and 9]. The referred limits were obtained from physical experiments using anthropomorphic dummies. In this figure, closed symbols correspond to overtopping flow observations, while the open symbols represent experiments conducted under constant flow conditions (floods).

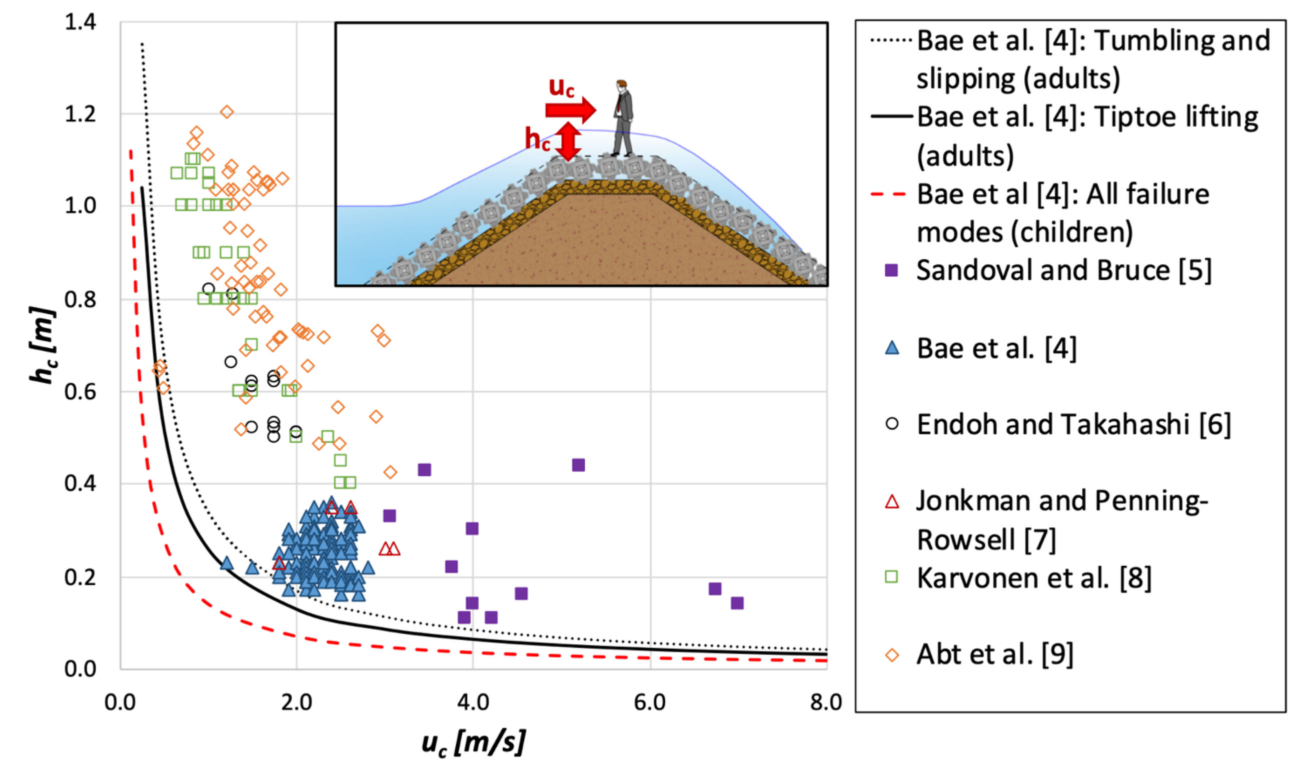

Fig. 1. Overtopping flow velocity, u_c and overtopping layer thickness, h_c limits for pedestrian stability given by Bae et al. [4] and other authors data.

The estimation of extreme OLT and OFV on breakwater crests is crucial to assess the hydraulic stability of the structure crest and pedestrian safety. Some studies in the literature are focused on the estimation of the OLT and OFV on dikes, but not on conventional mound breakwaters [10]. The objective of this study is to provide a method to estimate the OLT and OFV on conventional mound breakwaters during extreme overtopping events.

2. Literature review

Van Gent [11] proposed a method to estimate the wave run-up height exceeded by 2% of the incoming waves ($Ru_{2\%}$), estimated using Eqs. (1) to (4).

$$\begin{cases} \dfrac{Ru_{2\%}}{H_s} = c_0\,\xi_{s,-1} & if \quad \xi_{s,-1} \le p \\ \dfrac{Ru_{2\%}}{H_s} = c_1 - \dfrac{c_2}{\xi_{s,-1}} & if \quad \xi_{s,-1} \ge p \end{cases} \qquad \textbf{(1)}$$

where $c_0 = 1.35$, $c_1 = 4.0$, c_2 is given by Eq. (2), p is given by Eq. (3), $Ru_{2\%}$ is the wave run-up height exceeded by 2% of the incoming waves, $H_s=4(m_0)^{1/2}$ is the incident significant wave height at the toe of the structure, and $\xi_{s,-1}$ is the surf similarity parameter or Iribarren number given by Eq. (4), based on the spectral period $T_{m-1,0} = \frac{m_{-1}}{m_0}$, where m_i is the *i-th* spectral moment, $m_i = \int_0^\infty S(f) f_i df$, S(f) being the wave spectrum.

$$\boldsymbol{c_2 = 0.25\,\frac{{c_1}^2}{c_0}} \quad \textbf{(2)}$$

$$\boldsymbol{p = 0.5\frac{c_1}{c_0}} \quad \textbf{(3)}$$

$$\boldsymbol{\xi_{s,-1} = \frac{tan\,\alpha}{\sqrt{\frac{2\,\pi\,H_s}{g\,T^2_{m-1,0}}}}} \quad \textbf{(4)}$$

Later, Van Gent [12] and Schüttrumpf et al. [13] performed physical tests focusing on the measurement of OLT and OFV on dike crests. Subsequently, Schüttrumpf and Van Gent [14] integrated the results of the two studies and described the overtopping flow on the dike crest using two variables: (1) the OLT on the crest exceeded by 2% of the incoming waves, $h_{c,2\%}$, and the OFV on the breakwater crest exceeded by 2% of the incoming waves, $u_{c,2\%}$. Schüttrumpf and Van Gent [14] also proposed a method to estimate the OLT and the OFV on dike crests based on the wave run-up height exceeded by 2% of the incoming waves ($Ru_{2\%}$), estimated using Eqs. (1) to (4), given by Van Gent [11]. According to Schüttrumpf and Van Gent [13], $Ru_{2\%}$ is required to estimate the OLT and OFV on the seaside edge of the crest of the dike; $h_{A,2\%}(R_c) = h_A(z_A=R_c)$ and $u_{A,2\%}(R_c) = u_A(z_A=R_c)$. Fig. 2 shows the key parameters and variables considered in the model given by the aforementioned authors, where MWL is the mean water level.

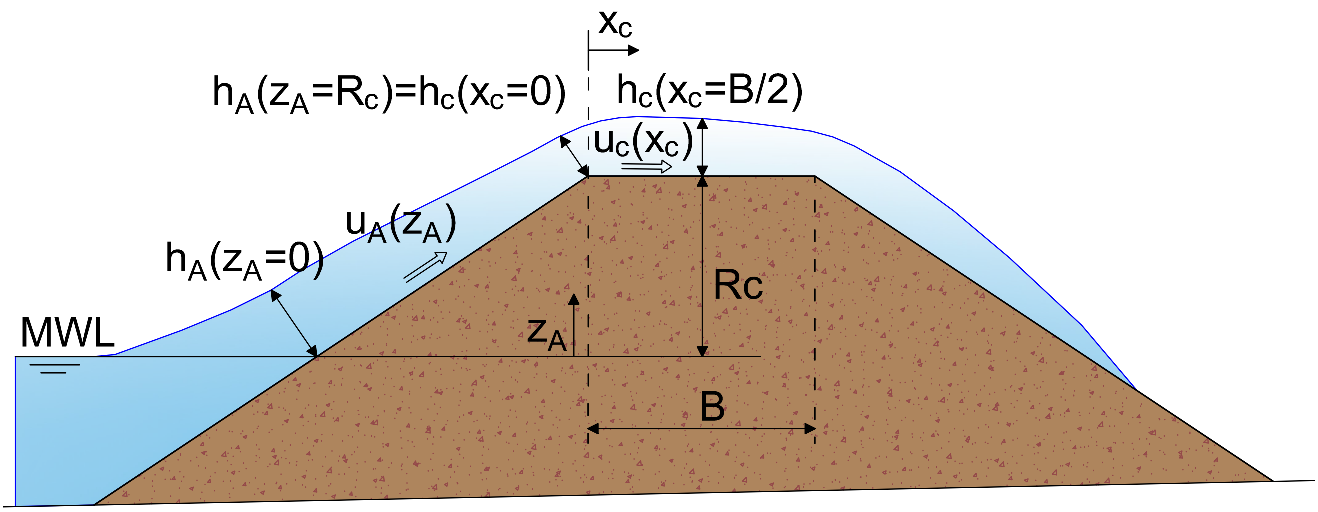

Fig. 2. Cross section defined by Schüttrumpf and Van Gent [14] to estimate overtopping layer thickness on dikes.

The OLT and OFV on the seaside slope of the dike ($0 \leq z_A \leq R_c$) can be estimated using Eq. (5) and Eq. (6), respectively.

$$\frac{h_{A,2\%}(z_A)}{H_s} = c^*_{A,h}\left(\frac{Ru_{2\%} - z_A}{H_s}\right) \tag{5}$$

$$\frac{u_{A,2\%}(z_A)}{\sqrt{g\,H_s}} = c^*_{A,u}\sqrt{\frac{Ru_{2\%} - z_A}{H_s}} \tag{6}$$

where $h_{A,2\%}(z_A)$ and $u_{A,2\%}(z_A)$ are the run-up layer thickness and velocity on the seaward slope exceeded by 2% of the incoming waves, respectively; z_A is the elevation on the MWL; $c_{A,h}{}^*$ and $c_{A,u}{}^*$ are the empirical coefficients given in Table 1.

According to Schüttrumpf and Van Gent [14], the formulas to estimate the OLT and OFV on the crest of the dike ($0 \leq x_c \leq B$) are, respectively:

$$\frac{h_{c,2\%}(x_c)}{h_{A,2\%}(R_c)} = exp\left(-c^*_{c,h}\,\frac{x_c}{B}\right) \tag{7}$$

$$\frac{u_{c,2\%}(x_c)}{u_{A,2\%}(R_c)} = exp\left(-c^*_{c,u}\,\frac{x_c\,\mu}{h_{c,2\%}(x_c)}\right) \tag{8}$$

where $h_{c,2\%}$ and $u_{c,2\%}$ are the overtopping layer thickness and overtopping flow velocity on the crest exceeded by 2% of the incoming waves, respectively; x_C is the distance to the intersection of the crest and seaward slope; B is the crest width; μ is a friction coefficient; $c_{c,h}^*$ and $c_{c,u}^*$ are the empirical coefficients given in Table 1. Schüttrumpf et al. [13] discussed the influence of the bottom friction coefficient, μ, on the OFV on the dike crest, and provided some guidelines for μ.

Regarding the empirical coefficients, Van Gent [12] and Schüttrumpf et al. [13] proposed different coefficients, based on their own experimental results. Table 1 shows relevant differences in coefficients $c_{A,h}^*$ and $c_{c,h}^*$ used in Eqs. (5) and (7), respectively, while minor differences can be observed for coefficients $c_{A,u}^*$ and $c_{c,u}^*$ used in Eqs. (6) and (8), respectively. The range of applicability for dikes when using these coefficients is also listed in Table 1.

Table 1. Range of applicability and empirical coefficients for dikes.

	Van Gent [12]	Schüttrumpf et al. [13]	Van der Meer et al. [16]
Slope (V/H)	1/4	1/3, 1/4, 1/6	1/3
R_c/H_s	0.7 - 2.2	0.0 - 4.4	0.7–2.9
H_s/h_s	0.2 – 1.4	0.1 – 0.3	0.1 – 0.3
$c_{A,h}^*$	0.15	0.33	0.13
$c_{A,u}^*$	1.30	1.37	-
$c_{c,h}^*$	0.40	0.89	-
$c_{c,u}^*$	0.50	0.50	-

The range of applicability of the empirical coefficients given by Van Gent [12] falls within the range of application of the coefficients given by Schüttrumpf et al. [13]. However, $h_{c,2\%}(B/2)$ calculated with Eqs. (5) and (7) using $c_{A,h}^*$=0.15 and $c_{c,h}^*$=0.40 proposed by Van Gent [12] is 58% ([0.15/0.33]×[exp(-0.40*1/2)/ exp(-0.89*1/2)]) of the $h_{c,2\%}(B/2)$ calculated with the same equations using $c_{A,h}^*$=0.33 and $c_{c,h}^*$=0.89 proposed by Schüttrumpf et al. [13]. Although the tested dikes were similar, the estimations of $h_{c,2\%}(B/2)$ given by Schuttrumpf et al. [13] are almost twice the estimations given by Van Gent [12]. Different experimental designs (e.g. bottom slope) and different experimental ranges (see, structure slope and R_c/H_s ranges in Table 1) may explain some differences. Further discussion on slope angle influence can be found in Bosman et al. [15]. Nevertheless, this significant difference is hard to explain because both refer to dikes in similar conditions.

Van der Meer et al. [16] conducted physical tests on a dike with a V/H = 1/3 slope and measured the OLT and OFV at the seaward crest edge, and at the landward crest edge. The range of variables in these tests is shown in Table 1.

Van der Meer et al. [16] combined their experimental results with the observations obtained by Van Gent [12] and Schüttrumpf et al. [13]. Based on this new data base, Van der Meer et al. [16] proposed a new method for dikes also based on the difference between the run-up height exceeded by 2% of the incoming waves, $R_{u,2\%}$, and the crest freeboard, R_c. Eq. (9) was proposed to estimate the OLT exceeded by 2% of the incoming waves at the seaward crest, $h_{A,2\%}(R_c)$. Considering $z_A=R_c$ in Eq. (5), Eq. (9) leads to $c_{A,h}^*=0.15$ given in Table 1. Eqs. (10) and (11) describe the OFV exceeded by 2% of the incoming waves at the seaward crest, $u_{A,2\%}(R_c)$, and the OFV decay along the crest, $u_{c,2\%}(x_c)$, respectively:

$$\boldsymbol{h_{A,2\%}(R_c) = 0.13\,(Ru_{2\%} - R_c)} \quad \textbf{(9)}$$

$$\boldsymbol{u_{A,2\%}(R_c) = 0.35\,\cot\alpha\,\sqrt{g\,(Ru_{2\%} - R_c)}} \quad \textbf{(10)}$$

$$\boldsymbol{\frac{u_{c,2\%}(x_c)}{u_{A,2\%}(R_c)} = exp\left(-1.4\frac{x_c}{L_{m-1,0}}\right)} \quad \textbf{(11)}$$

where α is the seaward slope angle, g is the gravity acceleration, and $L_{m-1,0}$ is the wave length based on the spectral period $T_{m-1,0}$. Van der Meer et al. [16] proposed a Rayleigh distribution to describe the distribution functions of the OLT and OFV.

Lorke et al. [17] performed physical model tests on dikes (V/H = 1/3 and 1/6), focusing on the effect of wind and currents on the overtopping on dikes with $0.33 \leq R_c/H_s \leq 2.86$ and $0.13 \leq H_s/h_s \leq 0.3$. These authors measured the OLT and OFV at the landward crest edge, using conventional wave gauges and miniature propellers. Based on their experimental observations, they proposed new values for the empirical coefficient $c_{c,h}^*$ of Eq. (7) given by Schüttrumpf and Van Gent [14] as a function of the seaside slope of the dike: $c_{c,h}^* = 0.35$ for V/H = 1/3 slope and $c_{c,h}^* = 0.54$ for V/H = 1/6 slope. It is noteworthy that these empirical coefficients were close to $c_{c,h}^* = 0.40$ proposed by Van Gent [12] for V/H=1/4.

Hughes et al. [18] analyzed the small-scale measurements on slightly submerged levees from Hughes and Nadal [19] within the range $-0.32 \leq R_c/H_s \leq -0.11$ and $R_c = -0.29$ m at the prototype scale (scale factor 1:25). During these tests, the OLT was measured on the crest close to the seaward side edge and landward edge using pressure cells, while the OFV was recorded using fiber-optic laser Doppler velocimeters at the same locations. From Eqs. (9) and (10) given by Van der Meer [16], Hughes et al. [18] derived a relationship between $h_{A,2\%}(R_c)$ and $u_{A,2\%}(R_c)$ and proposed the Eq. (12) using the landward side edge measurements:

$$\boldsymbol{u_{A,2\%}(z_A = R_c) = 1.53\sqrt{g\, h_{A,2\%}(z_A = R_c)}} \qquad \textbf{(12)}$$

Hughes et al. [18] also investigated the correlation between the OLT and OFV corresponding to the same overtopping event. No correlation was found between the OLT and OFV corresponding to the same overtopping event. Additionally, the distribution functions for the overtopping variables were studied and their coefficients were fitted utilizing the 10% upper values to better describe the most extreme overtopping events. The Rayleigh distribution was recommended to describe the OLT and OFV distributions.

EurOtop [1] proposed a method for dikes to estimate $h_{A,2\%}$ and $h_{c,2\%}$ based on the difference between the estimated wave run-up ($Ru_{2\%}$) and the crest freeboard (R_c). The OLT on the seaside slope edge of the dike, $h_{A,2\%}(R_c)$, was estimated by Eq. (5) using the coefficient $c_{A,h}^*$ given in Table 2. $Ru_{2\%}$, was estimated by Eqs. (13)

$$\boldsymbol{\frac{Ru_{2\%}}{H_s} = 1.65\ \gamma_f\, \gamma_\beta\, \gamma_b\, \xi_{s,-1}} \qquad \textbf{(13a)}$$

with a maximum value of

$$\frac{Ru_{2\%}}{H_s} = 1.0\,\gamma_f\,\gamma_\beta\left(4 - \frac{1.5}{\sqrt{\gamma_b\,\xi_{s,-1}}}\right) \tag{13b}$$

where γ_b is the influence factor for an existing toe berm, γ_f is the roughness factor, γ_β is the influence factor for oblique wave attack, and $\xi_{s,-1}$ is the breaker parameter given by Eq. (4). EurOtop [1] provided the roughness factors, γ_f.

Table 2. Empirical coefficient $c_{A,h}$* for Eq. (5) given by EurOtop [1].

Slope (V/H=1/3 and 1/4)	Slope (V/H=1/6)
0.20	0.30

Once $Ru_{2\%}$ is estimated using Eqs. (13), $h_{A,2\%}(R_c)$ is calculated using Eq. (5) with the coefficient $c_{A,h}^*$ given in Table 2. Finally, $h_{c,2\%}(x_C)$ is assumed to be constant after an initial turbulent zone and approximately equal to $h_{c,2\%}(x_C>>0)=(2/3)h_{A,2\%}(R_c)$ on the crest of the dike not close to the seaside slope.

3. Experimental Methodology

Two-dimensional small-scale physical tests were conducted in the wave flume (30 m × 1.2 m × 1.2 m) of the Laboratory of Ports and Coasts of the *Universitat Politècnica de València* (LPC-UPV), using a piston-type wavemaker and a gentle bottom slope (m = 1/50). Fig. 3 shows a longitudinal cross-section of the LPC-UPV wave flume as well as the location of the wave gauges utilized in this study.

The cross section of the model depicted in Fig. 4 corresponds to a mound breakwater with V/H = 2/3 slope and toe berms, protected with a single-layer Cubipod® armor, double-layer rock armor, and double-layer randomly-placed cube armor. In this study, the nominal diameters or equivalent cube sizes of the armor units were D_n = 37.9 mm for the Cubipod® units, D_n = 31.8 mm for rocks, and D_n= 39.7 mm for cubes. The range of variables in the tests is listed in Table 3; the test matrix is shown in Appendix A.

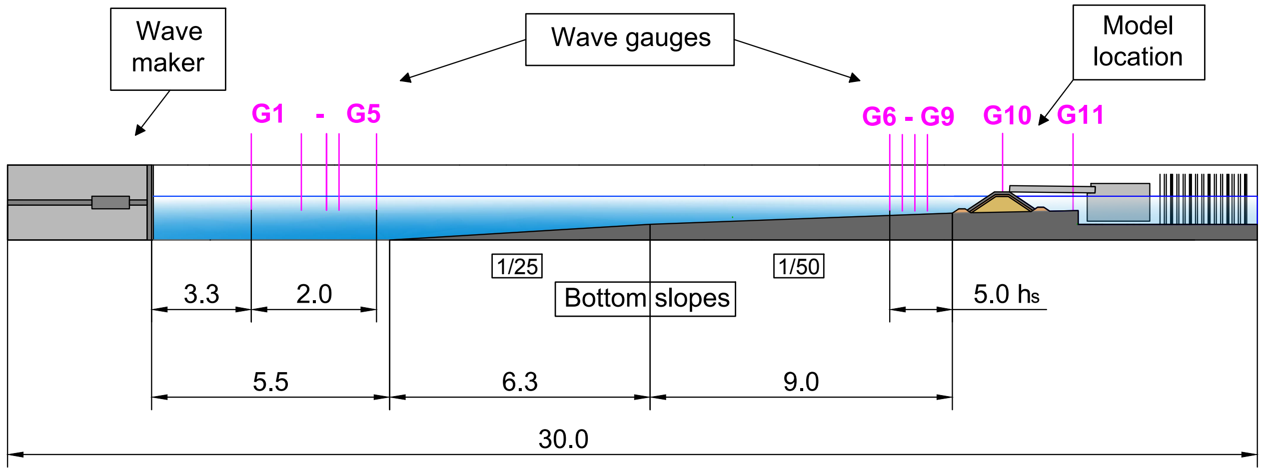

Fig. 3. Longitudinal cross section of the LPC-UPV wave flume (dimensions in meters).

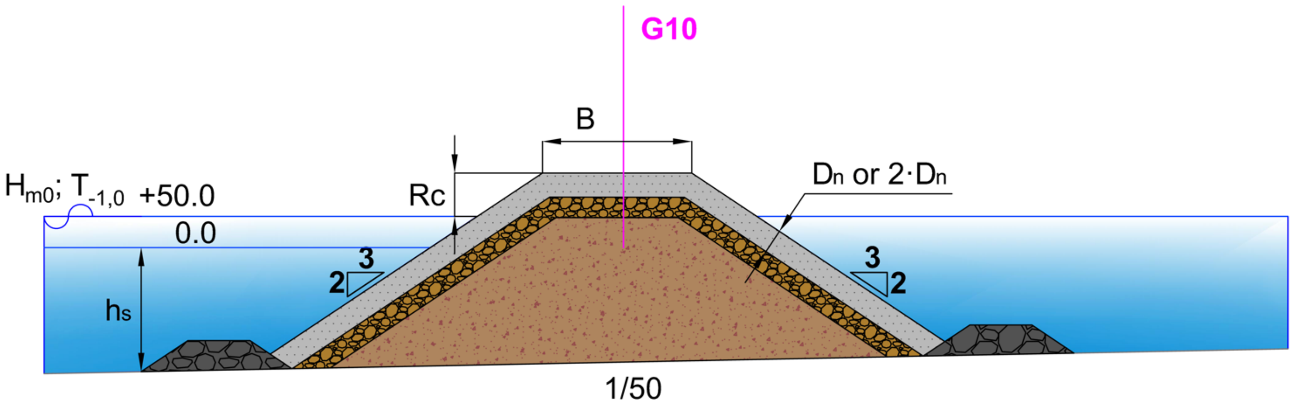

Fig. 4. Cross section of models tested in the LPC-UPV wave flume (dimensions in mm).

Table 3. Range of variables of 2D physical tests at the LPC-UPV wave fume.

	Cubipod® (1L)	Rock (2L)	Cube (2L)
R_c/H_s	0.43–1.38	0.80–1.75	0.34–1.67
H_s/h_s	0.30–0.73	0.29–0.61	0.20–0.64
H_s/D_n	0.15–0.19	0.13–0.16	0.13–0.16
B (mm)	240	259	265
D_n (mm)	37.9	31.8	39.7

One thousand random waves were generated following the JONSWAP spectra ($\gamma = 3.3$). The active wave absorption system AWACS was activated to avoid multireflections.

Each test series was associated to the water depth at the toe of the structure (h_s). For a given h_s, the significant wave height at the wave generation zone (H_{sg}) and peak period (T_p) were calculated such that the Iribarren number was maintained approximately constant along each test series of wave runs ($Ir_p=T_p/cot\alpha(2\pi H_{sg}/g)^{1/2}\approx$ 3 or 5). For each Iribarren number, Ir_p, the values of the significant wave height at the wave generating zone (H_{sg}) were increased, from no damage to failure of the armor layer, or wave breaking at the generation zone. H_{sg} was increased within the range $80 \leq H_{sg}(\text{mm}) \leq 240$ in steps of 10 mm. The water depth at the toe of the model was h_s= 200 and 250 mm for the Cubipod® and rock armored models, and h_s = 250 and 300 mm for the cube armored model. Owing to the importance of the crest freeboard of the structure when studying overtopping, two corrections have been considered: (1) the accumulated overtopping volumes extracted during the test series on a working day, and (2) the natural evaporation and facilities leakages that resulted in a small increase in the crest freeboard. The correction was 9.9 mm in the worst case. Neither pilling-up (wave gauge G11) nor low-frequency oscillations were significant during the tests.

The water surface elevation was measured using 11 capacitive wave gauges. Wave gauges G1 to G5 were placed close to the wavemaker following Mansard and Funke [20] recommendations, and were used to separate incident and reflected waves in the wave generation zone. Wave gauges G6 to G9 were located along the flume near the model, where depth-induced wave breaking occurs and existing methods to separate incident and reflected waves are not reliable. Wave gauge G10 was placed on the model crest and G11 was located behind the model. The distances from G6, G7, G8, and G9 to the toe of the model were varied with the water depth at the toe, h_s. G6, G7, G8, and G9 were placed at distances $5h_s$, $4h_s$, $3h_s$, and $2h_s$ from the toe of the structure, respectively, according to Herrera and Medina [21].

Armor damage was analyzed after each test by comparing the photographs captured perpendicular to the armor slope, using the Virtual Net method (Gómez-Martín and Medina [22]) in order to consider armor-unit extractions, sliding of the armor layer as a whole, and Heterogeneous Packing failure modes simultaneously (see Gómez-Martín and Medina [23]). Overtopping discharges were measured using a weighing system located in a collection tank behind the breakwater model during the test.

3.1. Measurement of overtopping layer thickness (OLT) and overtopping flow velocity (OFV)

As mentioned previously, the OLT was measured in the middle of the model crest using the capacitive wave gauge G10. These capacitive wave gauges must be partially submerged and they are calibrated with a certain reference level daily. To allow G10 to measure the OLT on the model crest, this wave gauge was introduced into a void vertical cylinder inserted in the model. This cylinder was 85 mm in diameter and 120 mm in length, and was filled up with water before the tests. Its upper part was closed with a lid covering the cylinder except for a slot to pass the wave gauge. Aeration was considered negligible because visual inspection of the overtopping events did not show significant aeration, but a clear water surface. The performance of the wave gauge G10 was excellent when measuring the OLT; low noise as well as low variations in the base level were observed (see Fig. 5). In this study, the maximum measured OLT of each overtopping event is considered the measured $h_c(B/2)$.

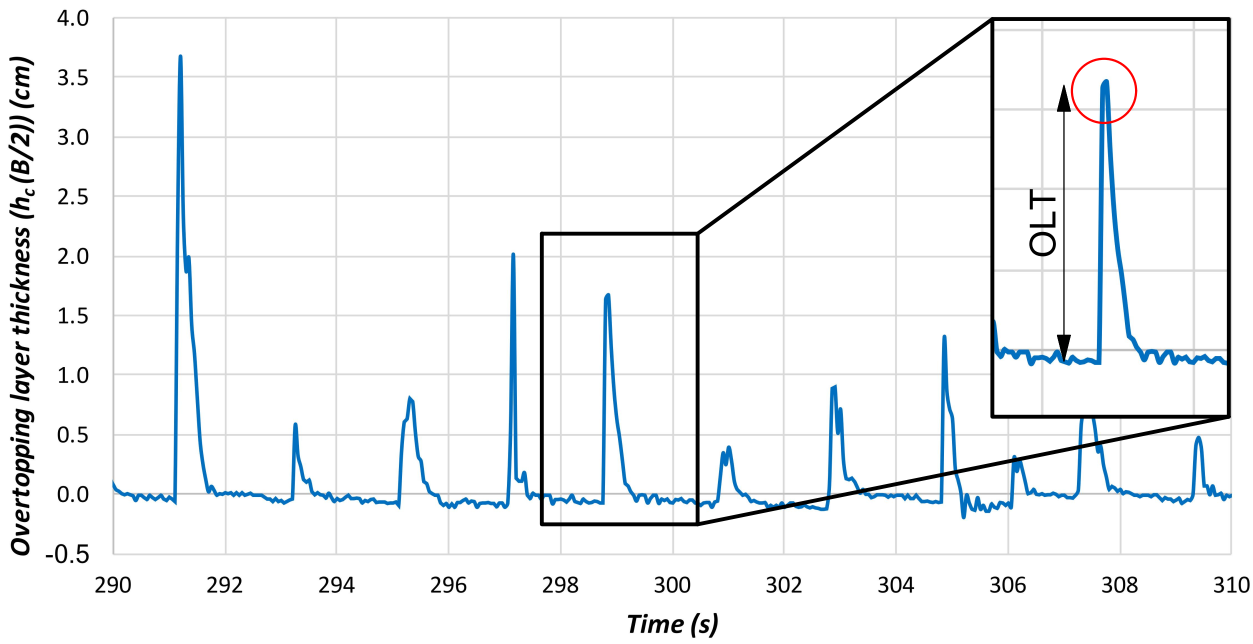

Fig. 5. Raw record of the OLT given by wave gauge G10.

The OFV were recorded in 66 out of 123 physical tests (13 tests with Cubipod®-1L armor, 14 test with rock-2L armor and 39 tests with cube-2L armor) using three miniature propellers installed on the model crest in three different positions: (1) seaward edge of the crest, (2) middle of the crest, and (3) landward edge of the crest. These propellers (11.6 mm in diameter) could measure the velocities within the range 0.15 m/s to 3.00 m/s. From the propeller measurements, the maximum measured values of the OFV of each overtopping event were obtained. Fig. 6 shows pictures of the aforementioned equipment.

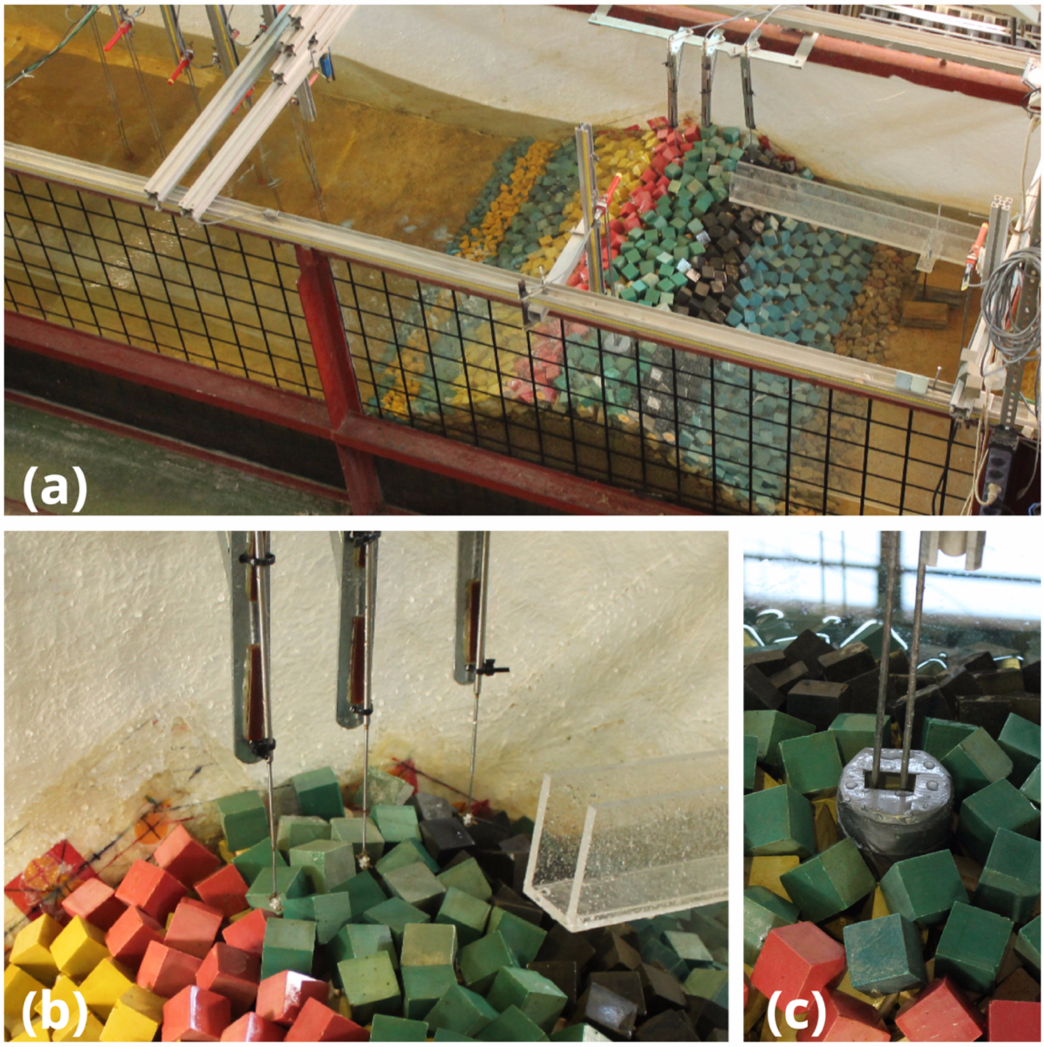

Fig. 6. Oblique view of the model in the LPC-UPV wave flume: (a) general view, (b) micro propellers and (c) wave gauge G10.

3.2. Wave analysis

Using wave gauges G1 to G5 located at the wave generation zone, incident and reflected waves were separated using the LASA-V method (see Figueres and Medina [24]). Although the LASA-V method is valid for nonlinear and nonstationary irregular waves, it is not valid for breaking waves. According to Battjes and Groenendijk [25], Composite Weibull distribution describes the wave height distribution on shallow foreshores. This distribution function is the one implemented in SwanOne software (see Verhagen et al., [26]). The incident significant wave height in the depth-induced breaking zone was estimated using the incident waves at the wave generation zone and the SwanOne numerical model (Verhagen et al. [26]). This methodology was validated by Herrera and Medina [21], who compared the numerical SwanOne estimations with measurements in the wave flume without any structure. A similar comparison was also performed in this study; the results are depicted in Fig. 7.

The relative Mean Squared Error (*rMSE*) given by Eq. (14) was used to measure the goodness of fit. $0 \leq rMSE \leq 1$ estimates the proportion of variance not explained by the prediction technique; therefore, the lower r*MSE*, the better are the predictions. In this case, *rMSE* = 4.1%.

$$\boldsymbol{rMSE = \frac{MSE}{VAR} = \frac{\frac{1}{N_o}\sum_{i=1}^{N_o}(t_i - e_i)^2}{\frac{1}{N_o}\sum_{i=1}^{N_o}(t_i - \bar{t})^2}} \qquad \textbf{(14)}$$

where MSE is the Mean Squared Error, VAR is the variance in the measured target values, N_o is the number of observations, t_i is the target value, e_i is the estimated value, and $\bar{t}$ is the average measured target value.

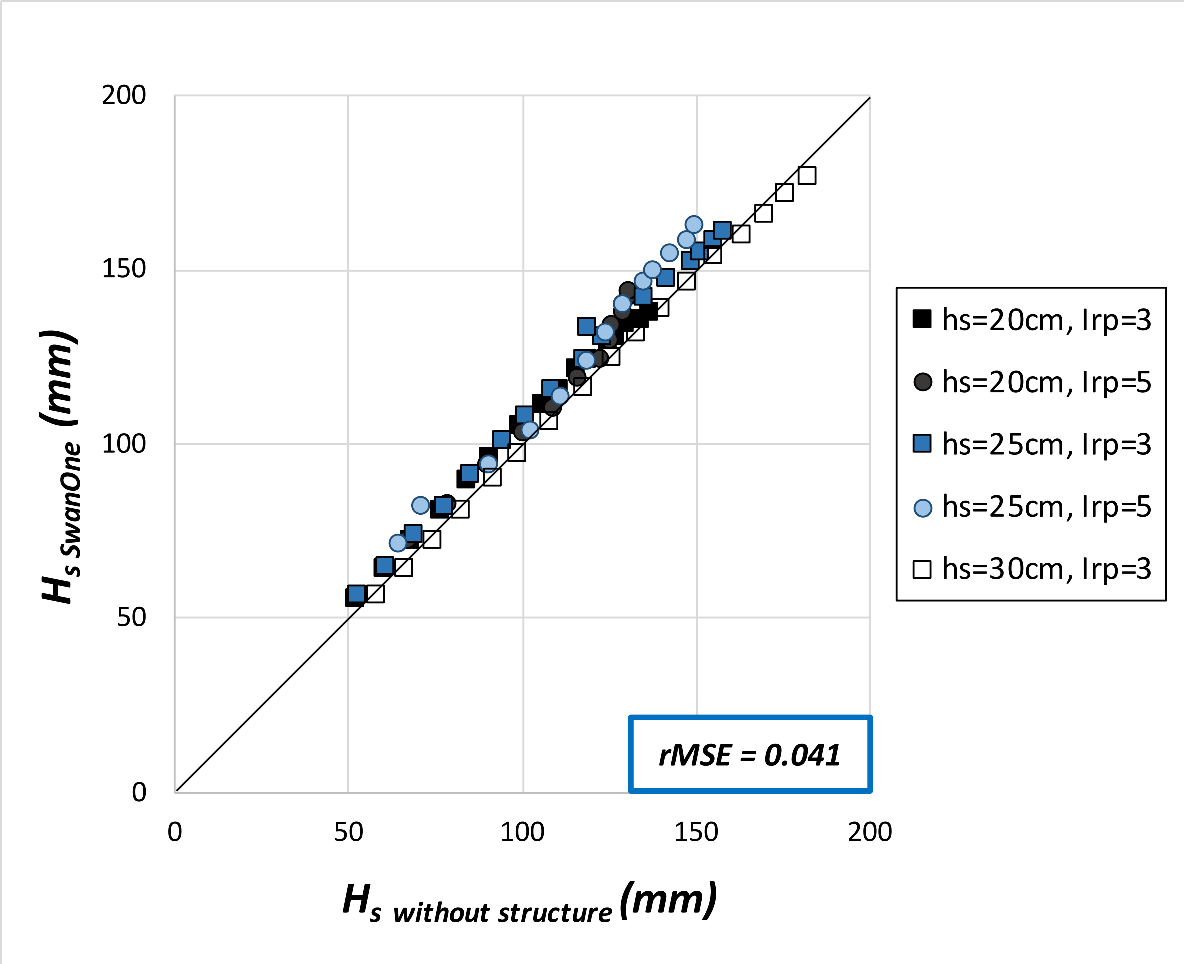

Fig. 7. Comparison of measured H_s without structure in the model zone and estimation given by SwanOne.

4. Comparison of the existing methods for estimating the overtopping layer thickness (OLT)

As mentioned in section 2, several methods are given in the literature to estimate the OLT exceeded by 2% of the incoming waves on the crest of a dike, $h_{c,2\%}$. Although they were proposed for dikes and not for conventional mound breakwaters, a comparison was performed between the OLT observed in this study on mound breakwater crests and the predictions by the aforementioned methods for dikes. To apply the EurOtop [1] formulas, the roughness factors recommended in the manual were used: γ_f= 0.49, γ_f= 0.40, and γ_f = 0.47 for single-layer Cubipod® armors, double-layer rock armored structures with a permeable core, and double-layer randomly-placed cube armors, respectively. However, it should be taken into account that Molines and Medina [27] pointed out that the roughness factors depend on the formula and experimental database; thus, γ_f should be calibrated specifically for each formula and database.

Fig. 8 compares the measured OLT exceeded by 2% of the incoming waves at the middle of the breakwater crest, $h_{c,2\%}(B/2)$, and the estimations given by Eqs. (5) and (7) (Schüttrumpf and Van Gent [14]) with coefficients $c_{A,h}^*$ and $c_{c,h}^*$ given in Table 1 (Van Gent [12], data in white, and Schüttrumpf et al. [13], data in blue) considering $Ru_{2\%}$ calculated with Eqs. (1) to (4) given by Van Gent [11]; and Eqs. (5) with coefficient $c_{A,h}^*$ given in Table 2 and $h_{c,2\%}(B/2)=(2/3)h_{A,2\%}(R_c)$, proposed by EurOtop [1], considering $Ru_{2\%}$ given in Eqs. (13) (EurOtop [1], data in red and black).

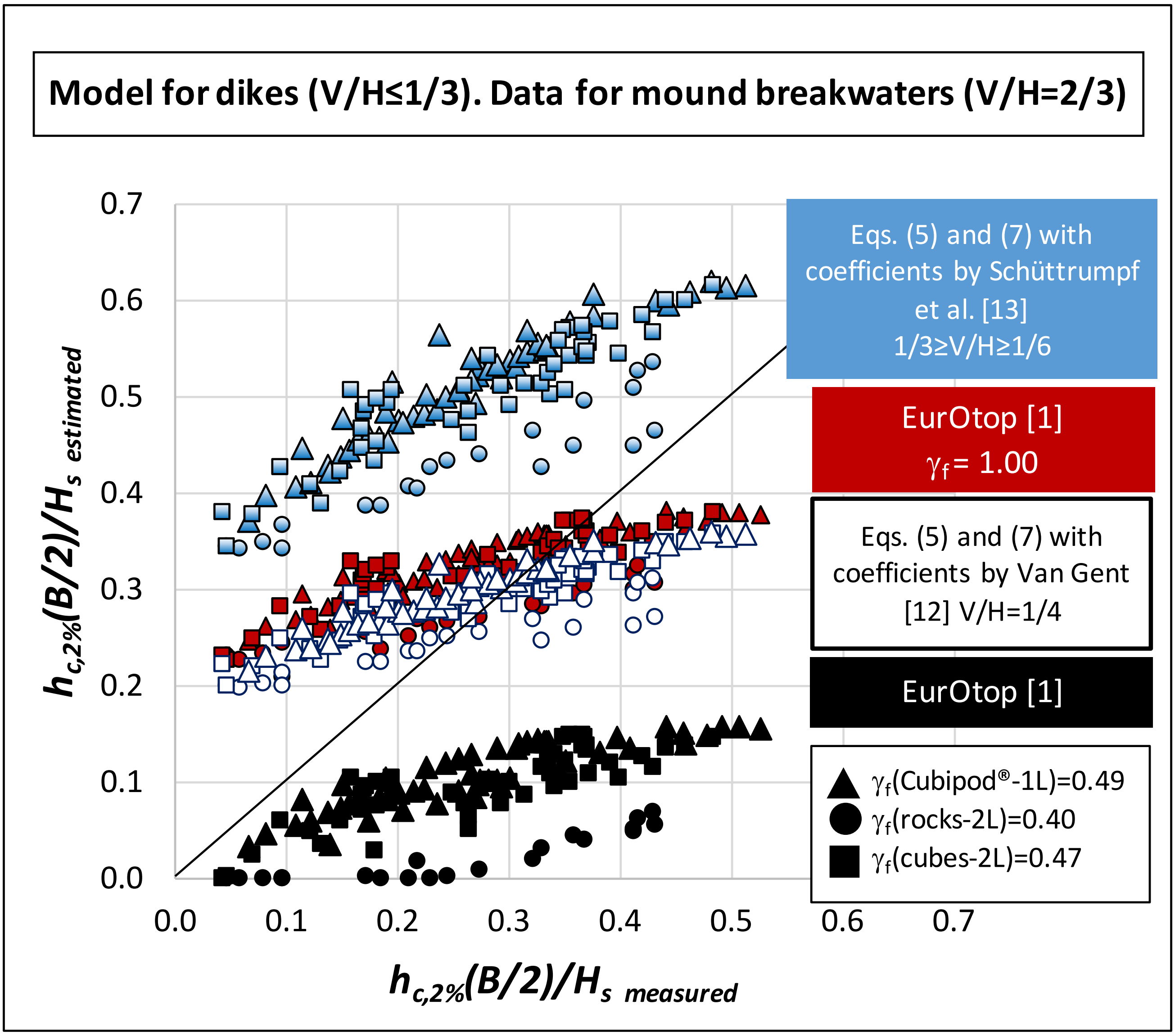

Fig. 8. Comparison of measured and estimated overtopping layer thickness, $h_{c,2\%}(B/2)$.

As mentioned in Section 2, estimations of $h_{c,2\%}(B/2)$ given by Eqs. (5) and (7) with coefficients $c_{A,h}^*$ and $c_{c,h}^*$ proposed by Schüttrumpf et al. [13] are almost twice the estimations obtained when considering the coefficients proposed by Van Gent [12], due the differences in the empirical coefficients shown in Table 1.

Using Eqs. (1) to (4) proposed by Van Gent [11] to estimate $Ru_{2\%}$ and $h_{c,2\%}(B/2)$ calculated using Eqs. (5) with $c_{A,h}^*$=0.20 and $h_{c,2\%}(B/2)=(2/3)h_{A,2\%}(R_c)$ proposed by EurOtop [1], $h_{c,2\%}(B/2)$ would be similar than that given by Eqs. (5) and (7) (Schüttrumpf and Van Gent [14]) with coefficients $c_{A,h}^*$=0.15 and $c_{c,h}^*$=0.40 proposed by Van Gent [12] (0.20/0.15×[(2/3)/exp(-0.40/2)]=1.09). As shown in Fig. 8, if Eqs. (13) proposed by EurOtop [1] with γ_f =1.00 are used to estimate $Ru_{2\%}$ (data in red), the estimation of $h_{c,2\%}(B/2)$ given by EurOtop [1] is also similar to that proposed by Van Gent [12]. However, if Eqs. (13) with γ_f proposed by EurOtop [1] are used to estimate $Ru_{2\%}$ (data in black), the estimation of $h_{c,2\%}(B/2)$ given by EurOtop [1] is much lower than $h_{c,2\%}(B/2)$ given by Van Gent [12].

To show the differences in estimating $Ru_{2\%}/H_s$ when roughness factors [1] are used, calculations are given for Test #1 in Table A.2. (double layer rock armored model). In this case, H_s= 104 mm, $T_{m-1,0}$ = 1.23s, $\gamma_\beta = \gamma_b = 1$, $\gamma_f = 0.40$ and $tan\alpha = 2/3$.

$\xi_{s,-1} = (2/3)/\sqrt{[(2 \times \pi \times 0.104)/(9.81 \times 1.23^2)]} = 3.18.$

Using Eqs. (1) to (4) proposed by Van Gent [11] with c_0 = 1.35 and c_1 = 4.0.

$c_2 = 0.25 \times 4.0^2/1.35 = 2.96$ and $p = 0.5 \times 4.0/1.35 = 1.48.$

$\xi_{s,-1} > p$ and $Ru_{2\%}/H_s = 4.0 - 2.96/3.18 = 3.07.$

Using Eqs. (13) proposed by EurOtop [1],

$Ru_{2\%}/H_s = 1.65 \times 1 \times 1 \times 0.40 \times 3.18 = 2.06$

With a maximum value of

$Ru_{2\%}/H_s = 1.0 \times 0.40 \times 1 \times \left(4 - 1.5/\sqrt{1 \times 3.18}\right) = 1.26$

$Ru_{2\%}/H_s$ (Van Gent [11]) = 3.07 >> 1.26 = $Ru_{2\%}/H_s$ (EurOtop [1])

None of the existing estimators for dikes compared in Fig. 8 represent the OLT on mound breakwaters satisfactorily. Furthermore, significant differences are found between some methods given in the literature for dikes.

5. A new method to estimate the overtopping layer thickness (OLT) on mound breakwater crests

5.1. OLT exceeded by 2% of the incoming waves, $h_{c,2\%}$ (B/2)

The formulas proposed by Schüttrumpf and Van Gent [14] and EurOtop [1] to estimate the OLT exceeded by 2% of the incoming waves on the crest of dikes (smooth impermeable slope) are not directly applicable to typical mound breakwaters (rough permeable slope where infiltration occurs). The methods proposed by EurOtop [1], Van Gent [12] and Schüttrumpf et al. [13] to calculate the OLT on the crest of the dikes are based on the estimation of $Ru_{2\%}$. In this study on mound breakwaters, it is reasonable to use Eqs. (15) to estimate $Ru_{2\%}$, as indicated by EurOtop [1] for mound breakwaters, calibrating the roughness factor γ_f to the formula and experimental observations recorded in this study.

$$\frac{Ru_{2\%}}{H_s} = 1.65\,\gamma_f\,\gamma_\beta\,\gamma_b\,\xi_{s,-1} \tag{15a}$$

with a maximum value of

$$\frac{Ru_{2\%}}{H_s} = 1.00\,\gamma_{f,surging}\gamma_\beta\,\gamma_b\left(4.0 - \frac{1.5}{\sqrt{\xi_{s,-1}}}\right) \tag{15b}$$

where $\gamma_{f,surging}$ [-] is a coefficient that increases linearly up to 1.0 following

$$\gamma_{f,surging} = \gamma_f + \left(\xi_{s,-1} - 1.8\right)\frac{1 - \gamma_f}{8,2} \tag{15c}$$

The maximum $Ru_{2\%}/H_s$ is 2.0 for permeable core. In this case, $\gamma_\beta = \gamma_b = 1$.

It is convenient to point out that roughness factors, γ_f, is a fitting parameter and γ_f is different depending on the formula and database [27]. It is also reasonable to use Eqs. (5) and (7) proposed by Schüttrumpf and Van Gent [14], calibrating the empirical coefficient $c_{A,h}^*$ with the experimental observations of this study.

Since OLT has been only measured in one site of the crest (x_C=$B/2$), $c_{c,h}^*$ cannot be calibrated in this study and the highest value of $c_{c,h}^*$ (maximum decay along the crest) found in the literature for dikes ($c_{c,h}^*$ = 0.89) is assumed. If $c_{c,h}^*$ was calibrated in the future (for mound breakwaters), the optimum $c_{A,h}^*$ given in Table 4 should be modified to keep constant $c_{A,h}^* \times exp(-c_{c,h}^*/2)$.

Considering a specific estimator and a given dataset, the *rMSE* could be used to estimate the optimum values of the roughness factors and empirical coefficients. However, no information would be obtained regarding the uncertainty of their estimations. Hence, a bootstrap resample technique was applied in this study to assess the uncertainty of the estimations. This technique consists of the random selection of N data from N original datasets. The probability of each datum to be selected each time is 1/N; therefore, some data were selected once, or more than once while some other data were absent in a resample.

First, using the results from 123 physical tests performed at the LPC-UPV wave flume, 1,000 resamples were performed optimizing both the roughness factors and the empirical coefficient $c_{A,h}^*$. Thus, 1,000 values of roughness factors and empirical coefficients that minimize the *rMSE* were obtained, and they were used to statistically characterize the parameters using percentiles 5%, 50%, and 95% (see Table 4).

Table 4. First level bootstrap resample results.

	P5%	P50%	P95%
$c_{A,h}^*$	0.49	0.52	0.54

Subsequently, the empirical coefficient value was fixed to their 50% percentile ($c_{A,h}^*$ = 0.52), and 1,000 bootstrap resamples were performed varying only the roughness factors, γ_f. The optimum roughness factors can be obtained for the model proposed using the 50% percentile for the empirical coefficients and the existing database. Using the obtained 1,000 values of each roughness factor, they were statistically characterized using the referred percentiles. Tables 4 and 5 show the results from both bootstrap resample levels.

Table 5. Second level bootstrap resample results using $c_{A,h}^* = 0.52$ and $c_{c,h}^* = 0.89$.

		P5%	P50%	P95%	rMSE
Roughness factor (γ_f)	Cubipod® (1L)	0.32	0.33	0.34	0.149
	Rock (2L)	0.46	0.48	0.50	0.183
	Cube (2L)	0.33	0.35	0.36	0.159

Fig. 9 shows the measured OLT at the middle of the breakwater crest, $h_{c,2\%}(B/2)$, as compared to the estimations given by Eqs. (15) and Eqs. (5) and (7) using the 50% percentile for the roughness factors and empirical coefficients given in Tables 4 and 5, as well as the 90% confidence interval. The *rMSE*, used to measure the goodness of fit, is given in Table 5.

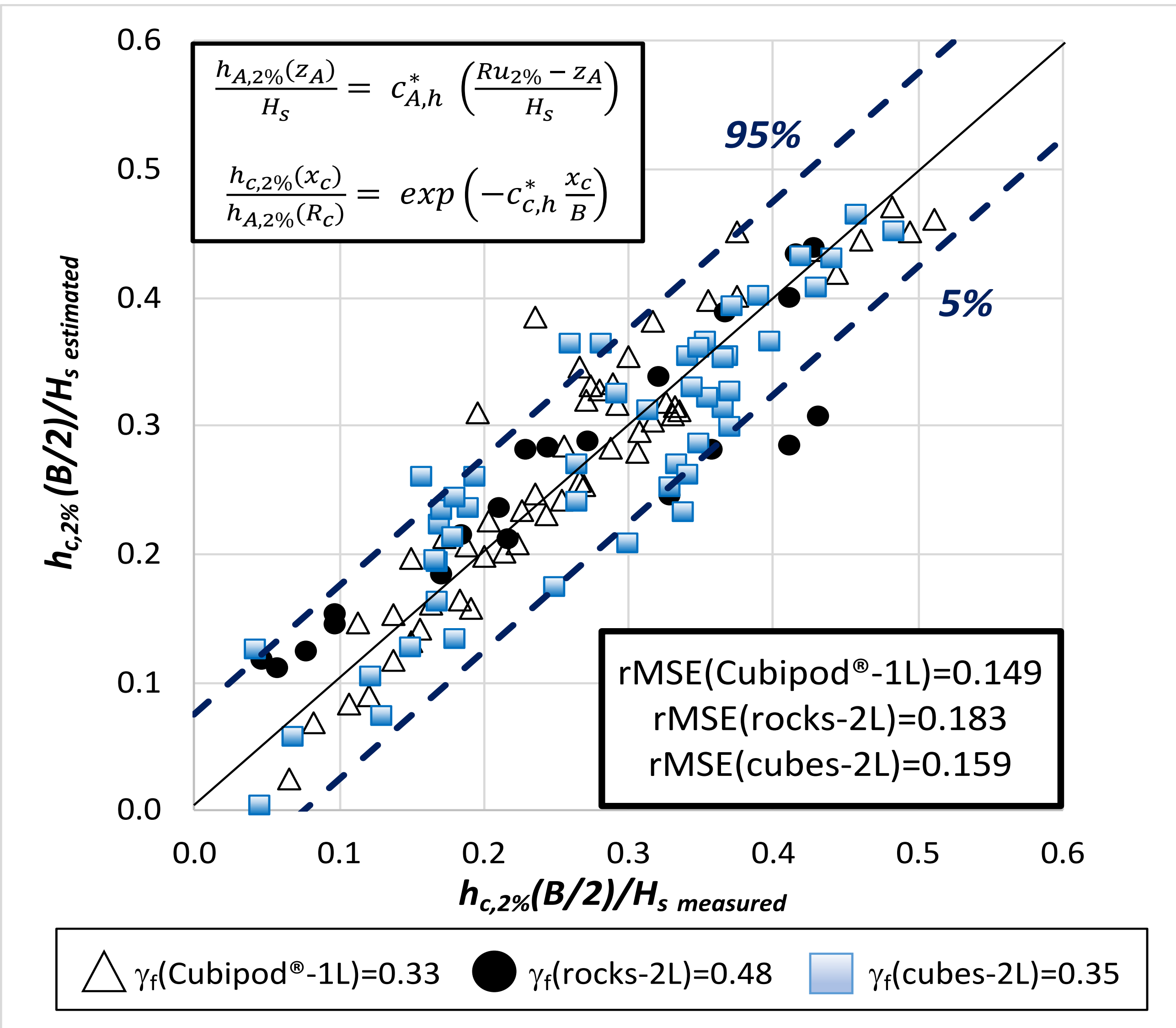

Fig. 9. Comparison of measured and estimated overtopping layer thickness, $h_{c,2\%}(B/2)$, and 90% confidence interval.

5.2. Distribution of OLT, $h_c\,(B/2)$

Extreme overtopping events are critical to assess the hydraulic stability of the breakwater crest and overtopping hazard to humans. Hence, it is necessary to describe not only the OLT exceeded by 2% of the incoming waves but also the OLT distribution in the most severe wave storms. As indicated by Hughes et al. [18], the extreme tail of the distribution of the overtopping variables is described better when only considering the low exceedance events. Therefore, in this study, only the OLT values associated with exceedance probabilities below 2% are used for calibration purposes.

As presented in section 2, in previous studies, a Rayleigh distribution was suggested for describing the overtopping variable distributions. Nevertheless, in this study, the best results were obtained with an Exponential distribution, given by Eq. (16).

$$F\left(\frac{h_c(B/2)}{h_{c,2\%}(B/2)}\right) = 1 - exp\left(-K_1\frac{h_c(B/2)}{h_{c,2\%}(B/2)}\right) \qquad (16)$$

where $h_c(B/2)$ is the value of the OLT with exceedance probabilities under 2%, $h_{c,2\%}(B/2)$ is the OLT not exceeded by 2% of the incoming waves, and K_1 is an empirical coefficient to be calibrated. K_1 is estimated for each physical test based on the 20 (1,000 × 2%) highest measured values of the OLT. The exceedance probability assigned to each OLT value was obtained as $m/(N+1)$, where m is the rank of the OLT observation and N the number of waves. Based on 2,460 (20 × 123) values obtained from 123 physical model tests, the best estimation is K_1 = 4.2. This coefficient was calculated as the 50% percentile of the 123 values that minimize the *rMSE* for each of the 20 OLT datasets. Fig. 10 shows the variability of the best fit values for K_1. Fig. 11 presents three example datasets of the proposed Exponential distribution in probability plot, while Fig. 12 shows the measured OLT distribution for each test against the proposed distribution, as well as the 90% confidence interval. As a result, *rMSE* = 0.162, indicating a good agreement with the experimental observations.

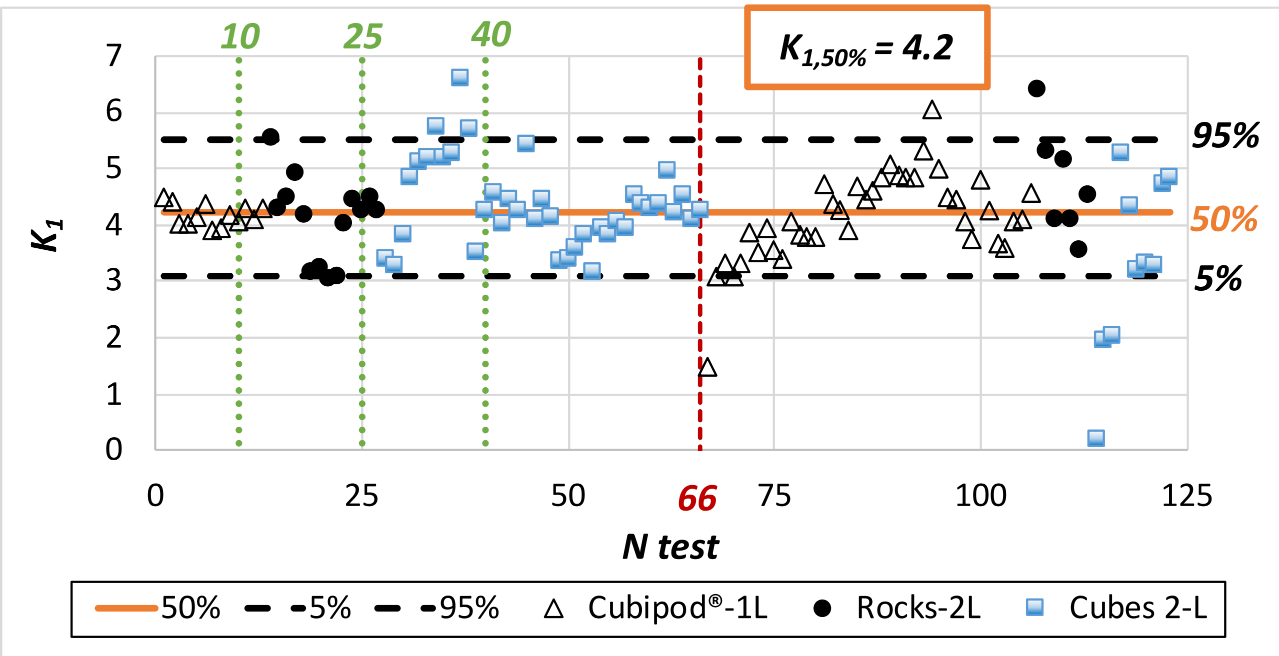

Fig. 10. 95%, 50%, and 5% percentile of K_1.

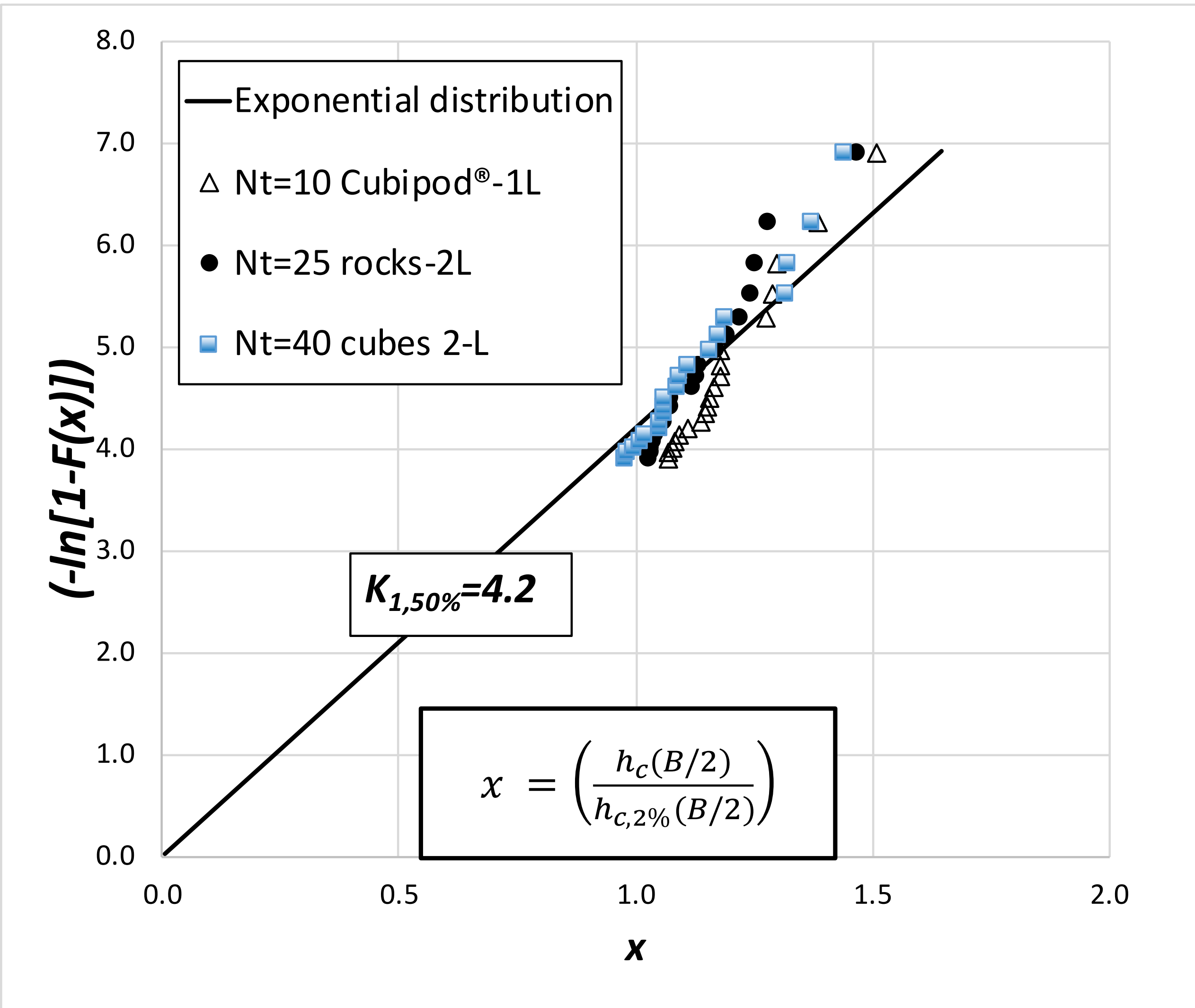

Fig. 11. Typical sample of cumulative distribution functions of OLT in equivalent probability plot.

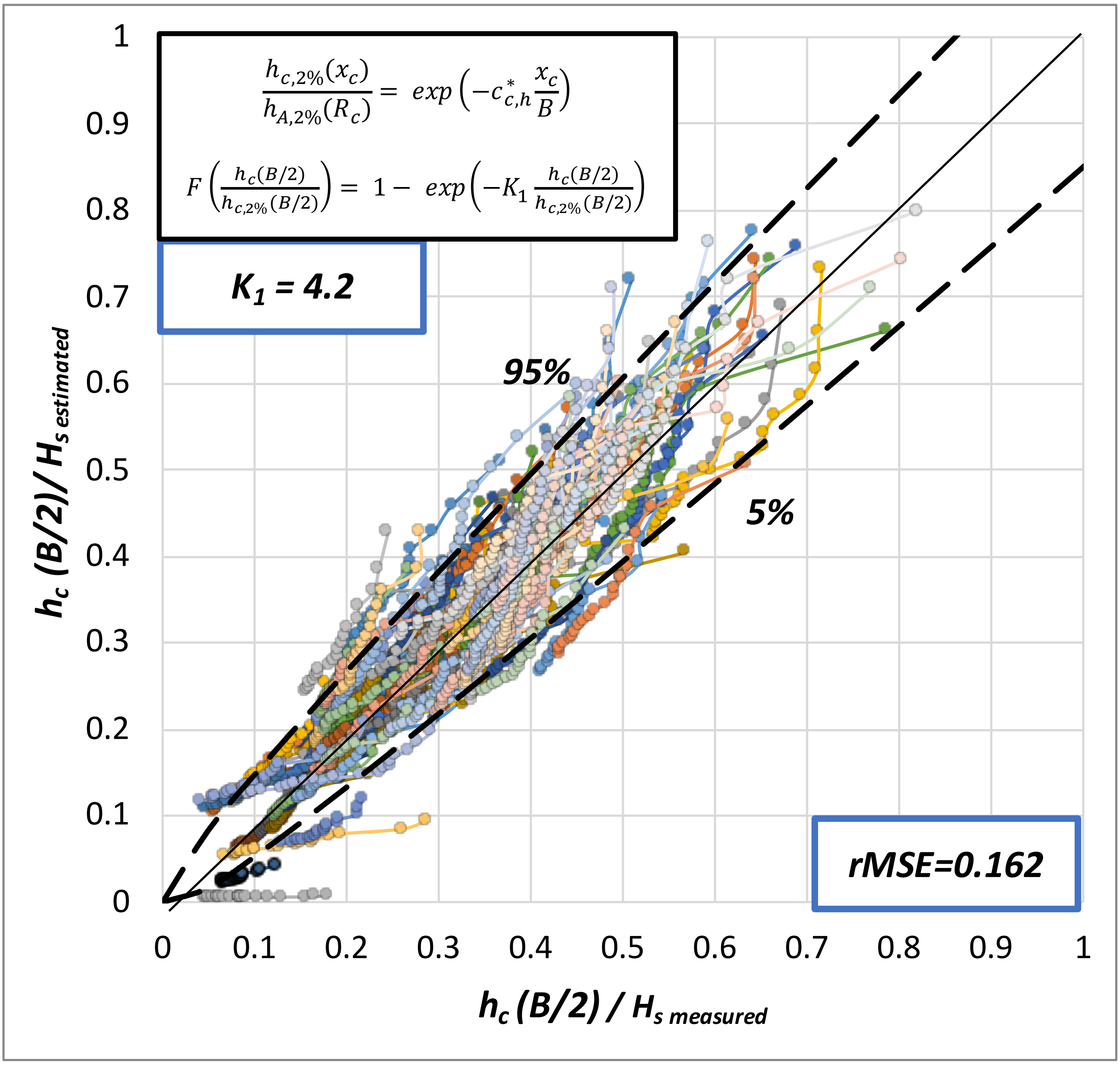

Fig. 12. Measured and estimated distribution of OLT in the middle of the breakwater crest, h_c *(B/2)*, for each test and 90% confidence interval.

6. A new method to estimate overtopping flow velocity (OFV) on mound breakwaters

6.1. OFV exceeded by 2% of the incoming waves, $u_{c,2\%}$ *(B/2)*

In section 2, different methods were presented to estimate the OFV exceeded by 2% of the incoming waves on the crest of a dike. Some of these proposals were based on the correlation between the statistics of the OLT and the statistics of the OFV (see Eqs. (8) and (12)). In this study, a new formula is proposed to estimate the OFV in the middle of the breakwater crest exceeded by 2% of the incoming waves, based on the relationship given by Eq. (17). It is noteworthy that the OLT exceeded by 2% of the incoming waves and OFV exceeded by 2% of the incoming waves do not always correspond to the same overtopping event.

$$\boldsymbol{u_{c,2\%}(B/2) = K_2\sqrt{g\, h_{c,2\%}(B/2)}} \qquad \textbf{(17)}$$

where $u_{c,2\%}(B/2)$ is the OFV at the middle of the breakwater crest exceeded by 2% of the incoming waves, K_2 is an empirical coefficient to be calibrated that depends on the armor unit, and $h_{c,2\%}(B/2)$ is the OLT at the middle of the breakwater crest exceeded by 2% of the incoming waves.

To obtain the best K_2 for each armor layer, the bootstrap resample technique was applied similarly to that described in section 4.1. Note that only the measured velocities within the operation range of the propellers (see section 3) have been used. First, 1,000 bootstrap resamples were created using the 66 OFV values. The optimum K_2 was determined for each sample as the one that minimizes the *rMSE*. Hence, 1,000 values of K_2 were obtained for each armor layer, such that they could be characterized statistically. The 5%, 50%, and 95% percentiles were used to this end and they are presented in Table 6 as well as *rMSE* values when using P50% of K_2. Fig. 13 compares the measured overtopping flow velocity exceeded by 2% of the incoming waves in the middle of the breakwater crest and the estimation given by Eq. (17) when using the 50% percentile of the K_2 coefficient.

Table 6. Statistical characterization of K_2 and *rMSE* values when using 50% percentile.

$\mathbf{K_2}$	P5%	P50%	P95%	rMSE
Cubipod® (1L)	0.56	0.57	0.59	0.228
Rock (2L)	0.46	0.47	0.49	0.114
Cube (2L)	0.57	0.60	0.63	0.233

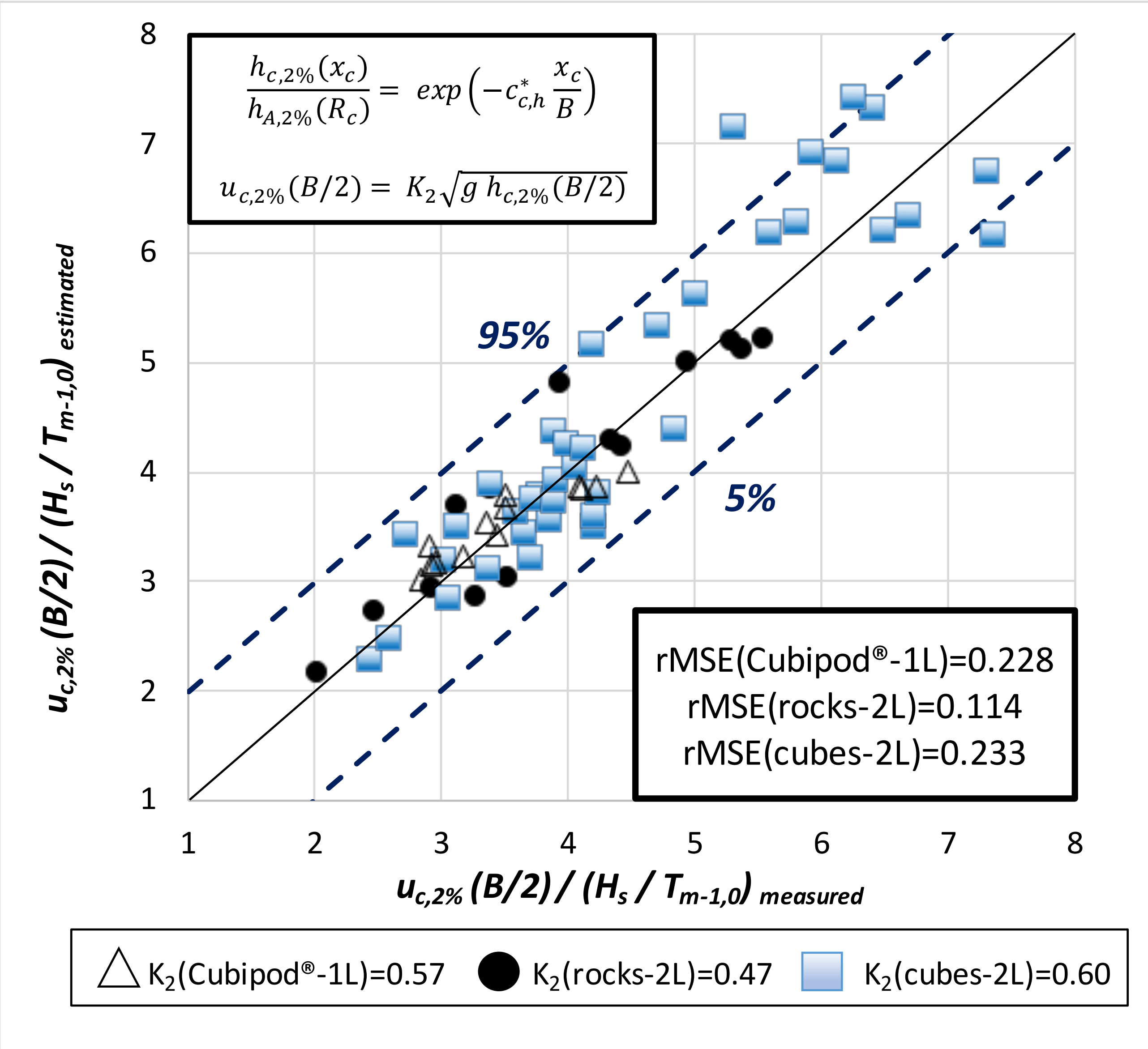

Fig. 13. Comparison of measured and estimated overtopping flow velocity, $u_{c,2\%}(B/2)$, and 90% confidence interval.

6.2. Distribution of OFV, u_c *(B/2)*

Eq. (17) shows a 1/2-power relationship between the OLT and OFV, and an Exponential distribution for the OLT has been proposed in section 5.2. Thus, a Rayleigh distribution is expected for the OFV, which is given by Eq. (18).

$$F\left(\frac{u_c(B/2)}{u_{c,2\%}(B/2)}\right) = 1 - exp\left(-K_3\left[\frac{u_c(B/2)}{u_{c,2\%}(B/2)}\right]^2\right) \quad \textbf{(18)}$$

where $u_c(B/2)$ is the value of the OFV with an exceedance probability under 2%, $u_{c,2\%}(B/2)$ is the OFV not exceeded by 2% of the incoming waves, and K_3 is an empirical coefficient to be calibrated. K_3 is estimated similarly as described in section 4.2. Based on 1,320 (66 × 20) values from 66 physical tests, the empirical coefficient is $K_3 = 3.6$, calculated as the value that minimizes the *rMSE*. The variability of K_3 values is presented in Fig. 14. Fig. 15 presents three example datasets of the proposed Rayleigh distribution in probability plot, while Fig. 16 compares the measured distribution of the OFV for each test versus the proposed distribution, as well as the 90% confidence interval.

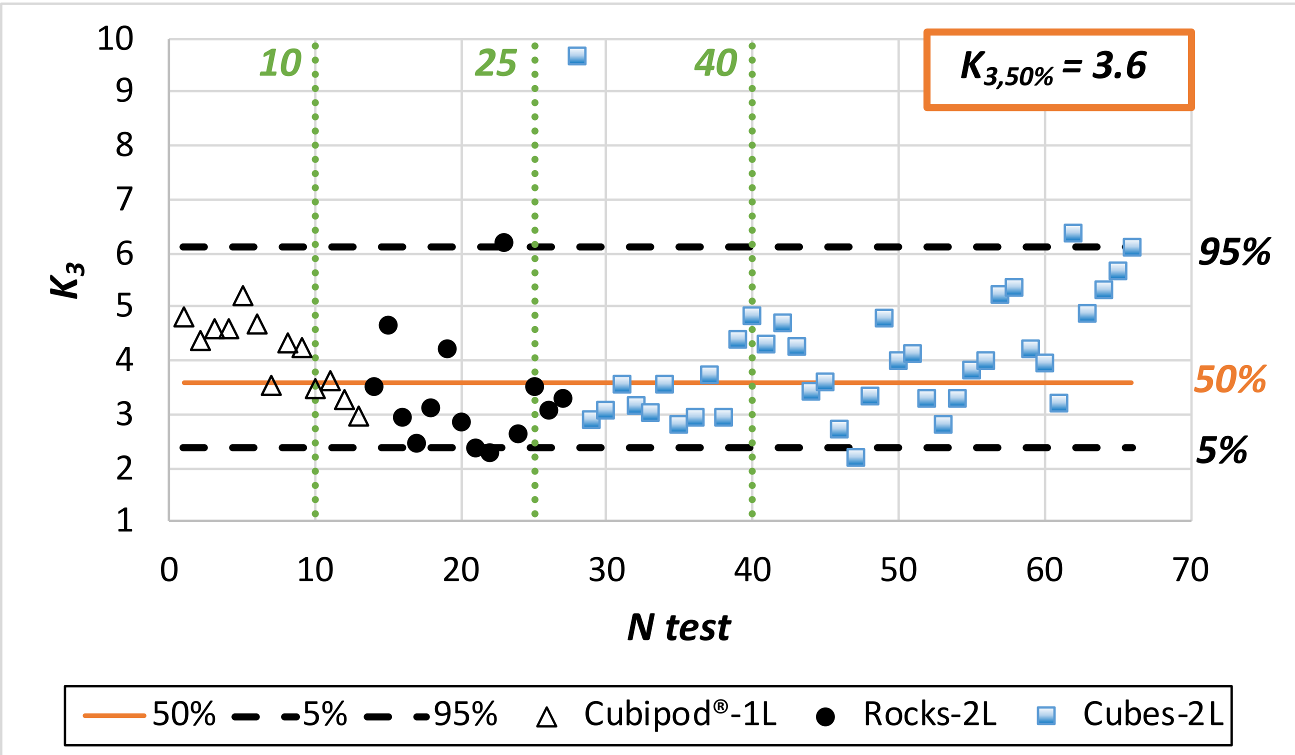

Fig. 14. 95%, 50%, and 5% percentile of K_3.

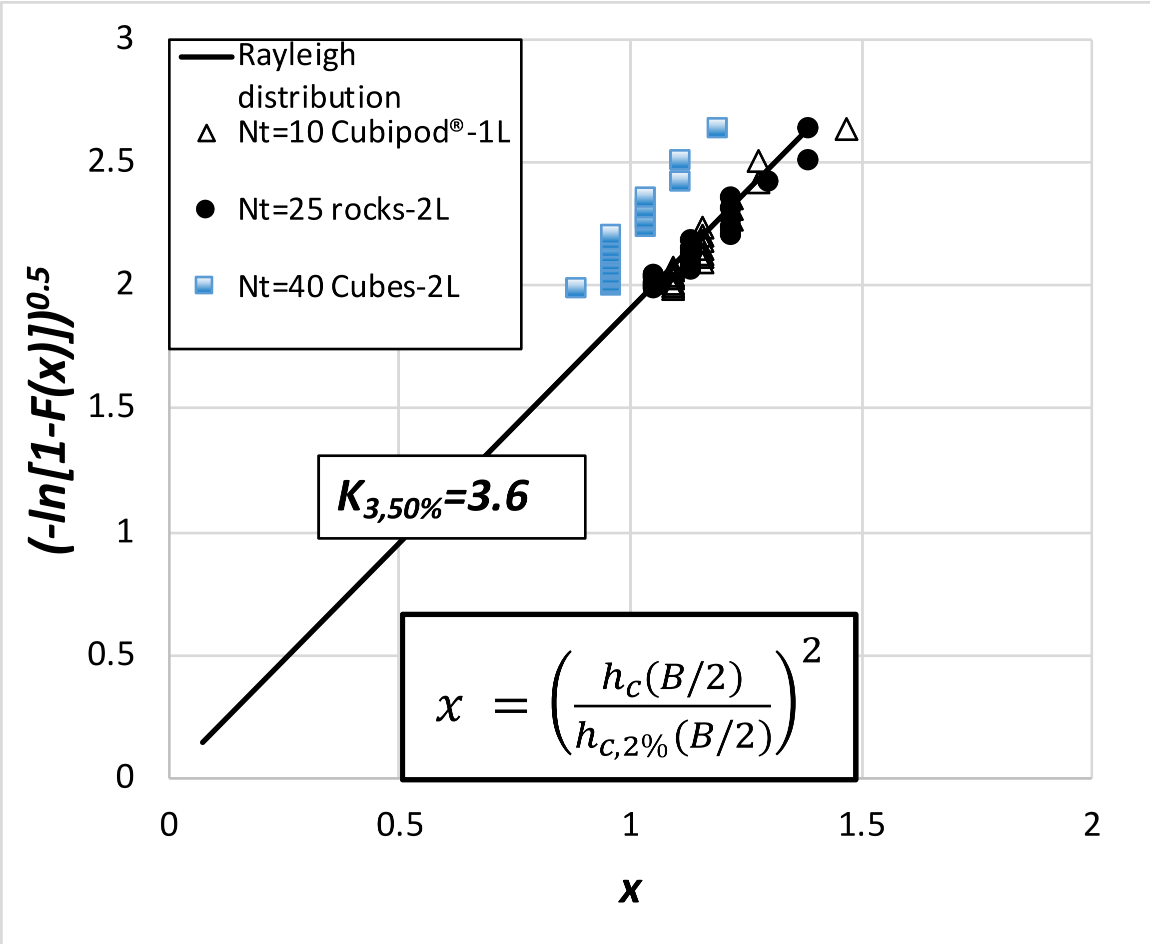

Fig. 15. **Typical sample of cumulative distribution function of OFV in equivalent probability plot.**

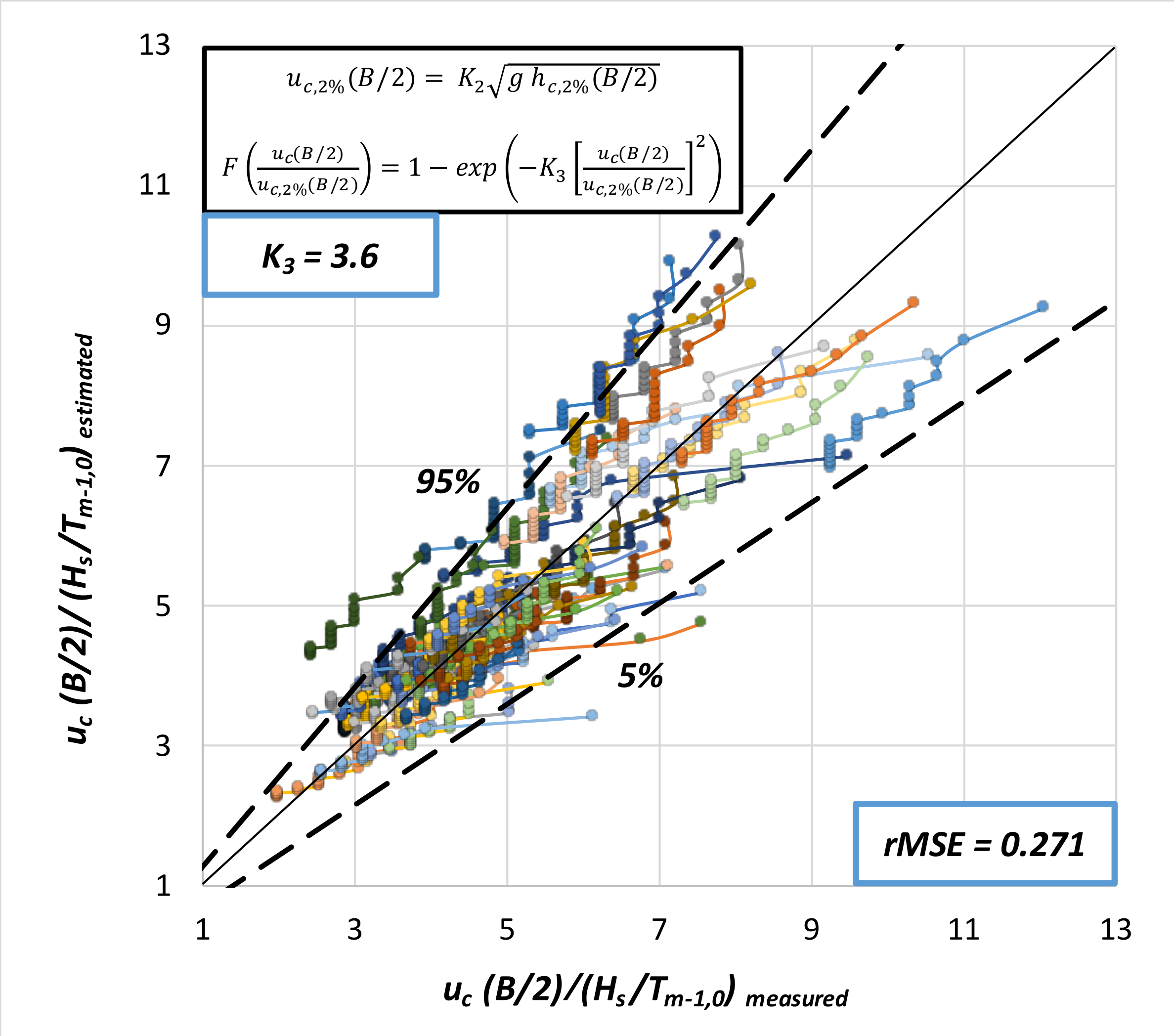

Fig. 16. Measured and estimated distribution of OFV in the middle of the breakwater crest, u_c *(B/2)*, and 90% confidence interval.

In this study, dimensionless OFV was $u_c(B/2)/(H_s/T_{m-1,0})$; $u_c(B/2)/(g\ H_s)^{0.5}$ and $u_c(B/2)/(g\ h_{c,2\%}(B/2))$ factors were also considered with poor results.

7. Relationship between overtopping layer thickness (OLT) and overtopping flow velocity (OFV) on mound breakwaters

In the previous sections, the statistics of the OLT and OFV were studied. However, the OLT and OFV values with the same exceedance probabilities may not correspond to the same overtopping event. Thus, in this section, the relationship between the OLT and OFV corresponding to the same overtopping event is studied. The highest 20 OLT values of each physical test (highest 2%) were selected, and the OFV values corresponding to the same overtopping event were determined, $h_c(B/2)$ and $u_{c,h}(B/2)$. The pairs of values where the velocity measurement is under 0.15 m/s were removed, as they were out of the operational range of the micro propellers (see section 3). Thus, not each physical test contains 20 pairs of $h_c(B/2)$ and $u_{c,h}(B/2)$. Fig. 17 shows the $h_c(B/2)$ values of each physical test compared to $u_{c,h}(B/2)$.

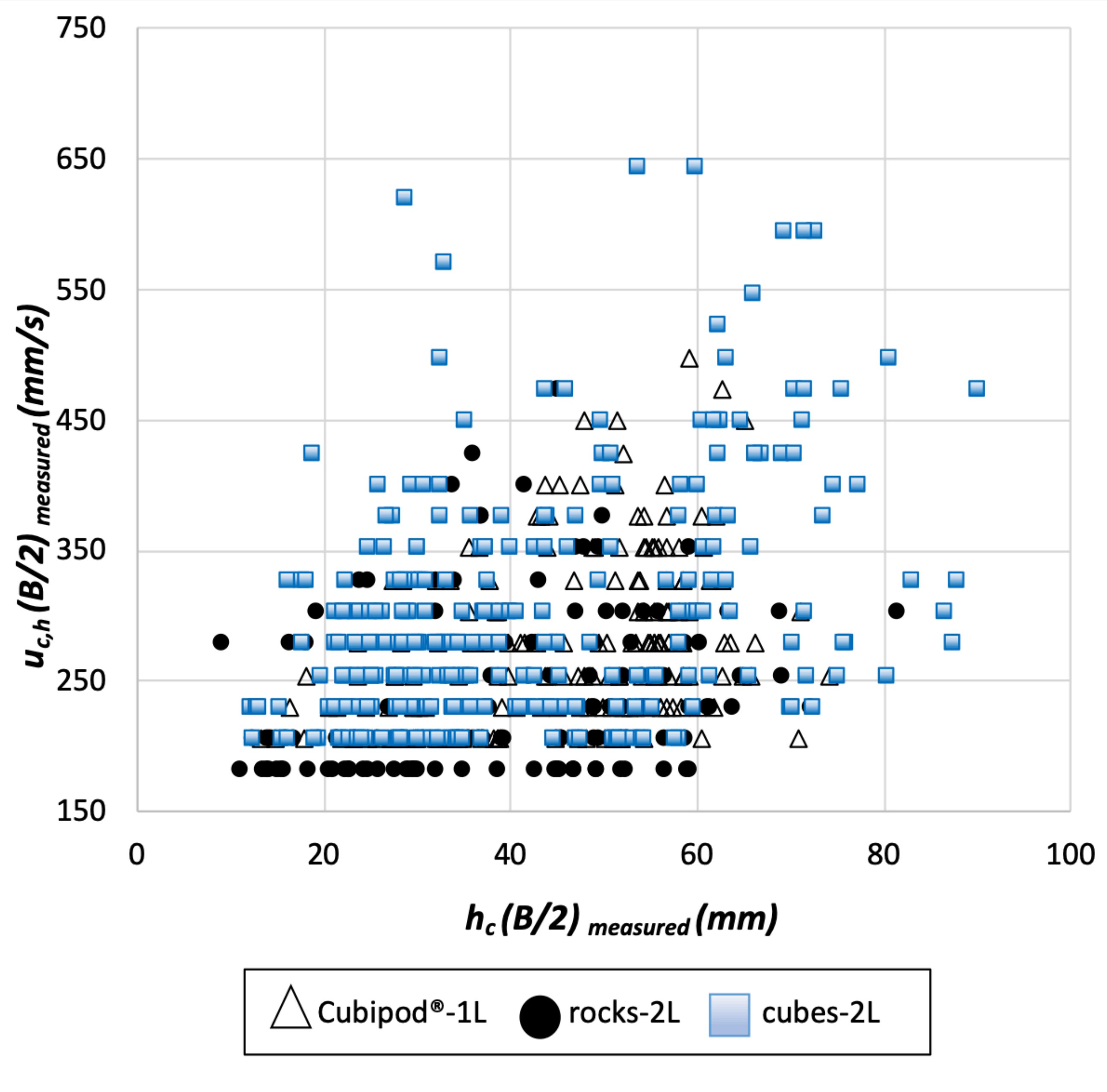

Fig. 17. Comparison of $h_c(B/2)$ and $u_{c,h}(B/2)$ corresponding to the same overtopping event.

Fig. 17 shows no clear correlation between measured $h_c(B/2)$ and $u_{c,h}(B/2)$. This result agrees with that of Hughes et al. [18], where no correlation was found between the OLT and OFV corresponding to the same overtopping event. It is noteworthy that the OLT and OFV (peak values) of the same overtopping event may not be simultaneous in time.

In this study, a statistical analysis was conducted to analyze the possible dependency of the OLT and OFV in the same overtopping event. In this case, the data were not Gaussian distributed; therefore, nonparametric statistical methods were used.

First, a hypothesis test based on the nonparametric Wald–Wolfowitz randomness test was used [28]. The null hypothesis (H_0) corresponds to the independency of the maximum values of the OLT, $h_c(B/2)$, and the OFV corresponding to the same overtopping event, $u_{c,h}(B/2)$. To apply the Wald–Wolfowitz randomness test, a minimum of eight pairs of values is required; therefore, it is applicable only to 47 physical tests. Using the level of significance of α = 0.10, H_0 was only rejected in five cases. The number of rejected cases has a binomial distribution with N = 47 and probability of rejection of the null hypothesis p = 0.1 (q = 0.9). The mean value is $Np = 4.7$ and the standard deviation is $\sqrt{Npq} = 2.1$. Using a significance level of α = 0.10, H_0 should be rejected only if the number of rejected tests is higher than seven cases (4.7 + 1.28 × 2.1); five (less than seven) rejected cases implies that the independence between $h_c(B/2)$ and $u_{c,h}(B/2)$ (H_0) is not rejected in this nonparametric test.

An additional nonparametric correlation test is proposed in this study to verify the independency of $h_c(B/2)$ and $u_{c,h}(B/2)$. This second test is based on the idea that if a significant correlation exists between $h_c(B/2)$ and $u_{c,h}(B/2)$ corresponding to the same overtopping event, the mean value of their product is significantly higher than the one obtained randomly reordering $u_{c,h}(B/2)$ within each test. In this hypothesis test, the H_0 corresponds to the independence between $h_c(B/2)$ and $u_{c,h}(B/2)$. A scheme of the test is depicted in Fig. 18.

The N highest OLT values of each physical test $h_c(B/2)_{i,j}$, with the corresponding OFV values, $u_{c,h}(B/2)_{i,j}$ were selected, where i = 1,...,66 is the test order number and j = 1,...≤20 is the data rank.

They were multiplied to obtain a fictitious overtopping discharge, $q_{i,j}$, and the average of these fictitious overtopping discharges within the same physical test was calculated $\bar{q}_i$. Subsequently, $u_{c,h}(B/2)_{i,j}$ values were randomly re-arranged within each test and associated to $h_c(B/2)_{i,j}$; this re-arrangement was repeated 100 times to obtain $(u_{c,h}(B/2)_{i,j})_k$, where k = 1,2,...,100 is the resample order number. New fictitious overtopping discharges were obtained, $(q_{i,j})_k$, and 100 new average fictitious overtopping discharges were calculated $(\bar{q}_i)_k$ for each physical test. Consequently, 6,600 (66 × 100) new average fictitious overtopping discharges $(\bar{q}_i)_k$ were obtained and compared to $\bar{q}_i$ obtained from the 66 tests without any re-arrangement.

If the OLT and OFV were correlated, $\bar{q}_i$ would be higher than $(\bar{q}_i)_k$ frequently. If $h_c(B/2)$ and $u_{c,h}(B/2)$ are independent (null hypothesis H_0), the number of cases where $\bar{q}_i > (\bar{q}_i)_k$ is a binomial distribution with N = 6,600, and the probabilities of acceptance and rejection of the hypothesis p = q = 0.5. The mean value is Np =3,300 and the standard deviation is $\sqrt{Npq} = 41$. The null hypothesis will be rejected if the number of cases with $\bar{q}_i > (\bar{q}_i)_k$ exceeds 3,352 (3,300 + 1.28 × 41), using a significance level α= 0.10. From 6,600 cases, only 3,172 (<3,352) cases have $\bar{q}_i > (\bar{q}_i)_k$. Subsequently, the H_0, i.e., independence between $h_c(B/2)$ and $u_{c,h}(B/2)$, is not rejected.

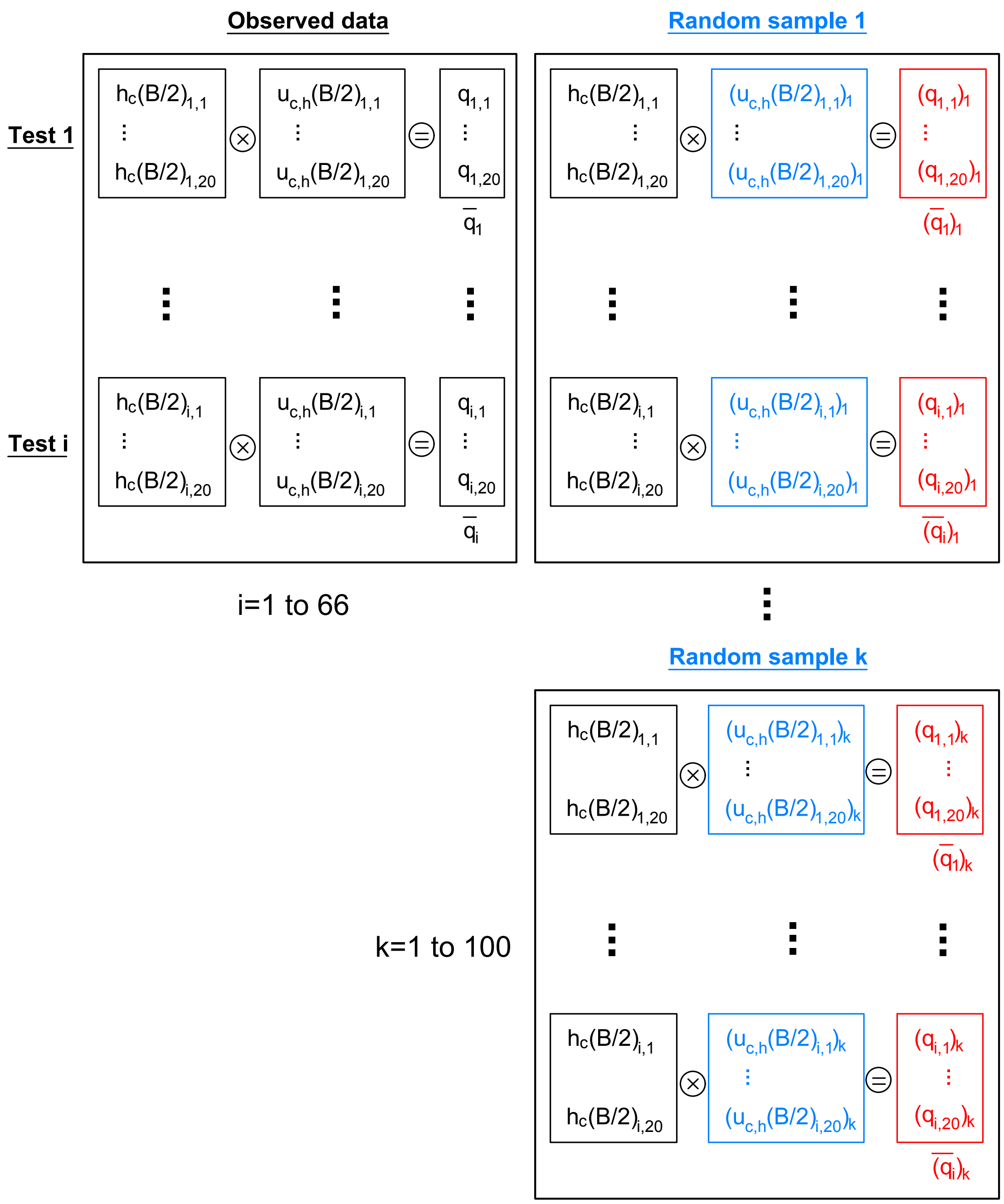

Fig. 18. Scheme of the correlation test.

According to these results, the OLT and OFV corresponding to the same overtopping event are not correlated. This implies that the wave conditions and structure geometry determine the magnitude of the overtopping event (see sections 4 and 5); therefore, the OLT and OFV statistics tend to increase or decrease with similar variables. Nevertheless, contrary to intuition, a relatively high OLT during a specific overtopping event do not necessarily correspond to a relatively high OFV, and vice versa.

8. Conclusions

The increasing social concern on the visual impact of coastal structures and climate change effects on the coast (e.g., sea level rise) tends to reduce the crest freeboards and increase overtopping rates. The overtopping hazard must be considered in the design and adaptation of the existing coastal structures. The mean overtopping rate is typically considered to design the crest of mound breakwaters. The OLT and OFV on the crest are also relevant for the hydraulic stability of the armored crest and rear side, as well as pedestrian safety when standing on the breakwater crest.

In this study, 123 physical tests of conventional mound breakwaters using a single-layer Cubipod® armor, a double-layer rock armor, and a double-layer randomly-placed cube armor were performed on the LPC-UPV wave flume. 66 tests measured both the OLT and OFV, while 57 additional tests measured only the OLT. The OLT on the model crest was measured with a conventional capacitance wave gauge, providing reliable measurements with a low level of noise. The OFV on the crest was measured using three miniature propellers.

A new method is proposed to estimate the OLT exceeded by 2% of the incoming waves at the middle of the breakwater crest, $h_{c,2\%}(B/2)$. It is based on Eqs. (15) to estimate the run-up $Ru_{2\%}$ proposed by EurOtop [1] for mound breakwaters, but using roughness factors calibrated with the experimental results given in this study: γ_f= 0.33 (Cubipod®-1L), 0.48 (rocks-2L), and 0.35 (cubes-2L). The new method estimated $h_{c,2\%}(B/2)$ with Eqs. (5) and (7) proposed by Schüttrumpf and Van Gent [14] for dikes, but using the empirical coefficients $c_{A,h}^* = 0.52$ and $c_{c,h}^* = 0.89$ calibrated in this study. The relative Mean Squared Error was $0.149 < rMSE < 0.183$.

To describe the OLT distribution at the middle of the breakwater crest $h_c(B/2)$ with exceedance probabilities under 2%, an exponential distribution function ($K_1 = 4.2$) was proposed, as shown in Eq. (16). K_1 was calibrated using experimental observations ($rMSE = 0.162$).

A new method was also proposed to estimate the OFV exceeded by 2% of the incoming waves at the middle of the breakwater crest, $u_{c,2\%}(B/2)$. The formula to estimate $u_{c,2\%}(B/2)$ is given by Eq. (17). The empirical coefficient of the proposed model was calibrated using the experimental observations for each armor layer: K_2 = 0.57 (Cubipod®-1L), 0.47 (rocks-2L) and 0.60 (cubes-2L): $0.114 < rMSE < 0.233$.

The OFV distribution with exceedance probabilities under 2%, $u_c(B/2)$, was described with a Rayleigh distribution function (K_3 = 3.6), according to Eq. (18). K_3 was calibrated with the experimental data ($rMSE$ = 0.271).

Finally, the correlation between OLT and OFV corresponding to the same extreme overtopping event was analyzed using two nonparametric tests. The statistics of the OLT and OFV were clearly related; however, contrary to intuition, the OLT and OFV values corresponding to the same overtopping event appeared to be independent; the null hypothesis of independence was not rejected at a significance level of 10%.

The results are valid for mound breakwaters ($0.34 \leq R_c/H_s \leq 1.75$) with armor slope V/H = 2/3 on a gentle sea bottom (m = 1/50).

Acknowledgements

The authors acknowledge the financial support from the *Ministerio de Economía y Competitividad* and the *Fondo Europeo de Desarrollo Regional (FEDER)* under grant BIA2015-70436-R, and from the *Conselleria d'Educació, Investigació, Cultura i Esport (Generalitat Valenciana)* under grant GV/2017/031. The first author was financially supported through the FPU program (*Formación de Profesorado Universitario*) funded by the *Ministerio de Educación, Cultura y Deporte* under grant FPU16/05081.

APPENDIX A. Test matrix

This appendix shows the test matrix used in this study. Wave runs of N_W=1,000 waves following a JONSWAP spectra ($\gamma = 3.3$) were generated. R_c is the crest freeboard, h_s is the water depth at the toe of the structure, H_{sg} is the significant wave height in the generation zone, $T_{m-1,0}$ is the spectral mean wave period, $H_s=4(m_0)^{1/2}$ is the significant wave height at the toe of the structure, $H_{1/10}$ is the average wave height of the highest tenth waves, $H_{2\%}$ is the wave height exceeded by 2% of the waves and $P_{OL}=N_{OL}/N_W$, where N_{OL} is the number of OLT events.

Test #	R_c (mm)	h_s (mm)	H_{sg} (mm)	$T_{m-1,0}$(s)	H_s (mm)	$H_{1/10}/H_s$ (-)	$H_{2\%}/H_s$ (-)	P_{OL}
1	120.4	200.4	99.8	1.14	92.3	1.38	1.51	5.0%
2	120.5	200.5	108.6	1.22	100.0	1.39	1.53	8.2%
3	120.6	200.6	117.5	1.23	106.2	1.40	1.54	15.7%
4	120.8	200.8	125.6	1.22	110.6	1.41	1.55	21.1%
5	121.3	201.3	134.5	1.29	117.1	1.42	1.56	27.4%
6	121.5	201.5	145.2	1.32	122.1	1.43	1.57	33.1%
7	121.6	201.6	152.6	1.35	125.2	1.44	1.58	39.4%
8	121.7	201.7	161.8	1.41	129.4	1.45	1.59	45.0%
9	121.9	201.9	168.7	1.42	130.7	1.45	1.59	50.1%
10	122.1	202.1	180.2	1.39	131.2	1.45	1.59	58.4%
11	122.3	202.3	189.4	1.54	136.0	1.46	1.60	61.0%
12	120.0	200.0	198.4	1.53	136.1	1.46	1.60	68.4%
13	120.4	200.4	206.5	1.56	136.9	1.46	1.60	68.9%
14	120.1	200.1	86.0	1.60	89.0	1.35	1.48	5.2%
15	120.3	200.3	97.9	1.73	102.5	1.40	1.54	13.1%
16	120.4	200.4	108.3	1.73	110.9	1.41	1.55	23.5%
17	120.6	200.6	117.4	1.79	117.9	1.43	1.57	34.9%
18	120.9	200.9	127.2	1.79	124.5	1.44	1.58	42.2%
19	121.3	201.3	136.9	1.91	131.5	1.45	1.59	52.4%
20	121.8	201.8	143.8	2.05	134.3	1.45	1.60	61.2%
21	122.6	202.6	153.5	2.06	137.7	1.46	1.61	68.0%
22	120.0	200.0	158.3	2.08	139.2	1.46	1.61	74.7%
23	121.0	201.0	167.1	2.09	141.2	1.47	1.61	77.1%
24	122.0	202.0	176.1	2.08	142.6	1.47	1.62	83.0%
25	123.2	203.2	184.8	2.21	145.0	1.47	1.62	86.4%
26	70.2	250.2	81.49	1.02	74.7	1.32	1.45	6.3%
27	70.3	250.3	90.75	1.13	84.7	1.33	1.47	12.1%
28	70.4	250.4	98.59	1.14	91.8	1.34	1.48	20.8%
29	70.4	250.4	108.82	1.21	101.7	1.36	1.49	29.3%
30	70.6	250.6	118.04	1.19	108.8	1.37	1.50	42.2%

Test #	R_c (mm)	h_s (mm)	H_{sg} (mm)	$T_{m-1,0}$(s)	H_s (mm)	$H_{1/10}/H_s$ (-)	$H_{2\%}/H_s$ (-)	P_{OL}
31	70.7	250.7	126.89	1.22	116.2	1.38	1.52	54.6%
32	71.0	251.0	136.09	1.27	124.3	1.39	1.53	65.6%
33	71.3	251.3	145.16	1.37	132.7	1.40	1.54	73.8%
34	71.8	251.8	152.58	1.36	137.9	1.41	1.55	83.9%
35	72.8	252.8	162.74	1.44	143.6	1.42	1.56	87.6%
36	73.8	253.8	173.02	1.49	149.3	1.43	1.57	98.9%
37	75.0	255.0	182.62	1.52	153.8	1.43	1.58	100.0%
38	76.7	256.7	192.63	1.58	158.3	1.44	1.58	100.0%
39	78.2	258.2	198.21	1.57	159.2	1.44	1.58	100.0%
40	79.9	259.9	205.67	1.60	161.3	1.45	1.59	100.0%
41	71.3	251.3	76.27	1.55	76.5	1.32	1.45	11.9%
42	71.6	251.6	87.19	1.65	88.6	1.34	1.47	26.6%
43	70.0	250.0	95.99	1.76	99.7	1.36	1.49	38.8%
44	70.3	250.3	106.51	1.75	110.2	1.37	1.51	54.3%
45	70.8	250.8	114.58	1.83	118.4	1.38	1.52	65.1%
46	71.9	251.9	125.29	1.87	128.8	1.40	1.54	82.9%
47	70.0	250.0	133.68	2.01	136.9	1.41	1.55	100.0%
48	71.9	251.9	142.18	2.11	144.6	1.42	1.56	98.6%
49	74.0	254.0	150.71	2.00	148.7	1.43	1.57	100.0%
50	70.0	250.0	160.75	2.09	154.0	1.43	1.58	100.0%
51	70.3	250.3	168.62	2.17	158.0	1.44	1.58	100.0%
52	70.6	250.6	177.19	2.14	161.7	1.45	1.59	100.0%
53	71.3	251.3	181.92	2.24	164.4	1.45	1.59	100.0%
54	120.0	200.0	62.78	0.91	57.0	1.31	1.44	<2%
55	120.2	200.2	71.75	1.00	65.9	1.33	1.46	<2%
56	120.3	200.3	80.79	1.03	74.3	1.35	1.48	<2%
57	120.3	200.3	90.65	1.14	84.8	1.37	1.50	<2%
58	120.0	200.0	75.22	1.54	77.3	1.35	1.48	<2%
59	70.0	150.0	62.13	0.96	56.7	1.29	1.42	<2%
60	70.1	150.1	72.71	0.94	66.1	1.31	1.44	<2%

Table A. 1. Test matrix for single-layer Cubipod® armored model.

Test #	R_c (mm)	h_s (mm)	H_{sg} (mm)	$T_{m-1,0}$(s)	H_s (mm)	$H_{1/10}/H_s$ (-)	$H_{2\%}/H_s$ (-)	P_{OL}
1	151.4	200.3	113.9	1.23	103.9	1.40	1.54	6.40%
2	151.8	200.7	121.9	1.22	108.5	1.41	1.55	7.90%
3	151.1	200.0	130.9	1.27	114.9	1.42	1.56	12.80%
4	151.3	200.2	83.5	1.60	86.9	1.37	1.50	3.20%
5	151.3	200.2	94.2	1.73	99.3	1.39	1.53	8.80%
6	151.5	200.4	104.6	1.73	108.0	1.41	1.55	18.20%
7	151.9	200.8	113.2	1.79	116.5	1.42	1.56	29.60%
8	152.1	201.0	121.8	1.79	121.9	1.43	1.57	37.90%
9	102.1	251.0	79.0	1.02	72.5	1.32	1.45	2.30%
10	101.1	250.0	87.8	1.13	81.2	1.33	1.46	5.64%
11	101.7	250.6	96.6	1.14	89.7	1.34	1.47	9.83%

Test #	R_c (mm)	h_s (mm)	H_{sg} (mm)	$T_{m-1,0}$(s)	H_s (mm)	$H_{1/10}/H_s$ (-)	$H_{2\%}/H_s$ (-)	P_{OL}
12	101.1	250.0	104.6	1.21	97.3	1.35	1.49	19.54%
13	101.2	250.1	115.5	1.19	108.1	1.37	1.50	26.14%
14	101.3	250.2	123.8	1.22	113.9	1.38	1.51	36.33%
15	101.7	250.6	130.5	1.27	120.5	1.39	1.52	43.50%
16	101.1	250.0	74.2	1.55	74.4	1.32	1.45	6.30%
17	101.2	250.1	84.8	1.65	86.2	1.34	1.47	15.80%
18	101.4	250.3	95.4	1.76	99.2	1.36	1.49	30.10%
19	101.1	250.0	105.2	1.75	109.0	1.37	1.50	51.40%
20	101.2	250.1	111.9	1.83	117.2	1.38	1.52	60.40%
21	101.3	250.2	122.5	1.87	126.6	1.39	1.53	69.50%
22	151.1	200.0	62.7	0.89	57.0	1.31	1.44	<2%
23	151.4	199.7	71.1	1.00	65.4	1.33	1.46	<2%
24	151.7	199.5	79.7	1.00	73.1	1.34	1.48	<2%
25	151.1	200.0	86.9	1.10	80.7	1.36	1.49	<2%
26	151.2	199.9	96.5	1.16	89.8	1.37	1.51	<2%
27	151.3	199.8	105.0	1.20	97.0	1.39	1.52	<2%
28	151.1	200.0	73.1	1.54	75.2	1.35	1.48	<2%
29	101.1	250.0	60.4	0.91	55.1	1.29	1.42	<2%
30	101.6	249.6	69.4	0.96	63.3	1.30	1.43	<2%

Table A. 2. Test matrix for double-layer rock armored model.

Test #	R_c (mm)	h_s (mm)	H_{sg} (mm)	$T_{m-1,0}$(s)	H_s (mm)	$H_{1/10}/H_s$ (-)	$H_{2\%}/H_s$ (-)	P_{OL}
1	111.7	249.4	81.7	1.09	75.6	1.32	1.45	2.8%
2	111.9	249.2	91.0	1.16	84.9	1.33	1.47	4.4%
3	112.0	249.1	97.9	1.15	91.2	1.34	1.48	7.3%
4	112.3	248.8	107.9	1.19	100.3	1.36	1.49	10.6%
5	112.4	248.7	116.4	1.21	108.1	1.37	1.50	14.0%
6	111.1	250.0	126.1	1.29	117.3	1.38	1.52	21.8%
7	111.3	249.8	137.1	1.37	127.0	1.40	1.53	27.1%
8	111.5	249.6	146.4	1.36	132.4	1.40	1.54	32.5%
9	111.8	249.3	155.0	1.45	140.0	1.41	1.55	36.9%
10	112.1	249.0	163.4	1.49	145.2	1.42	1.56	41.9%
11	112.5	248.6	175.3	1.49	150.0	1.43	1.57	48.9%
12	112.9	248.2	182.2	1.52	153.6	1.43	1.58	51.8%
13	111.1	250.0	186.6	1.57	156.5	1.44	1.58	55.8%
14	111.5	249.6	190.4	1.57	157.6	1.44	1.58	58.0%
15	111.1	250.0	69.3	1.55	69.5	1.31	1.44	2.2%
16	111.6	249.6	80.2	1.70	82.3	1.33	1.46	6.4%
17	111.9	249.2	91.7	1.72	94.7	1.35	1.48	12.9%
18	112.0	249.1	101.2	1.77	105.1	1.36	1.50	22.1%
19	111.1	250.0	107.9	1.95	114.3	1.38	1.51	30.7%
20	111.5	249.6	118.3	1.88	123.0	1.39	1.53	44.8%
21	111.9	249.2	126.9	2.04	132.1	1.40	1.54	52.9%
22	112.4	248.7	135.5	2.08	139.7	1.41	1.55	61.5%

Test #	R_c (mm)	h_s (mm)	H_{sg} (mm)	$T_{m-1,0}$(s)	H_s (mm)	$H_{1/10}/H_s$ (-)	$H_{2\%}/H_s$ (-)	P_{OL}
23	113.2	247.9	141.5	2.08	144.0	1.42	1.56	100.0%
24	114.6	246.5	151.2	2.10	148.7	1.43	1.57	80.3%
25	116.1	245.0	162.0	2.24	155.3	1.44	1.58	87.4%
26	111.1	250.0	173.4	2.25	160.9	1.44	1.59	92.3%
54	61.2	299.9	72.7	0.91	66.8	1.29	1.42	2.4%
28	61.3	299.8	81.7	0.97	74.9	1.30	1.43	8.7%
29	61.4	299.7	89.3	1.04	82.4	1.31	1.44	16.1%
30	61.5	299.6	98.9	1.09	91.8	1.32	1.45	21.9%
31	61.9	299.2	107.6	1.12	99.9	1.33	1.46	27.7%
32	62.1	299.0	115.6	1.18	108.4	1.34	1.47	29.4%
33	62.2	298.9	124.2	1.23	114.8	1.35	1.48	32.6%
34	62.5	298.6	131.8	1.13	123.5	1.36	1.50	34.4%
35	62.7	298.4	137.3	1.28	128.7	1.37	1.50	38.4%
36	63.2	297.9	147.0	1.34	138.3	1.38	1.51	41.2%
37	63.7	297.4	154.7	1.40	143.3	1.38	1.52	43.8%
38	61.1	300.0	164.7	1.38	151.6	1.39	1.53	50.3%
39	62.5	298.6	173.4	1.55	160.0	1.40	1.54	50.3%
40	64.0	297.1	180.9	1.54	163.8	1.41	1.55	48.9%
41	65.8	295.3	190.1	1.55	169.0	1.42	1.56	45.8%
42	68.4	292.7	199.4	1.62	175.1	1.42	1.56	47.2%
43	61.1	300.0	70.5	1.54	69.5	1.29	1.42	10.0%
44	61.2	299.9	81.1	1.65	80.9	1.31	1.44	21.5%
45	61.3	299.8	90.8	1.76	92.5	1.32	1.45	34.5%
46	62.0	299.1	99.6	1.77	101.6	1.33	1.47	43.3%
47	62.7	298.4	108.6	1.92	112.9	1.35	1.48	59.9%
48	61.1	300.0	116.6	1.90	120.7	1.36	1.49	72.6%
49	62.0	299.1	126.0	2.05	131.5	1.37	1.51	82.2%
50	111.1	250.0	54.4	0.95	49.6	1.28	1.41	<2%
51	111.3	249.8	62.6	0.95	57.0	1.29	1.42	<2%
52	111.1	250.0	72.9	1.04	66.9	1.31	1.44	<2%
53	61.1	300.0	64.3	0.91	59.0	1.28	1.41	<2%

Table A. 3. Test matrix for double-layer cube armored model.

References

[1] EurOtop, 2018. *Manual on wave overtopping of sea defences and related structures*. An overtopping manual largely based on European research, but for worldwide application. Van der Meer, J.W., Allsop, N.W.H., Bruce, T., De Rouck, J., Kortenhaus, A., Pullen, T., Schüttrumpf, H., Troch, P. And Zanuttigh, B., www.overtopping-manual.com.

[2] Argente, G., Gómez-Martín, M.E., Medina, J.R., 2018. Hydraulic Stability of the Armor Layer of Overtopped Breakwaters. *Journal of Marine Science and Engineering 2018, 6(4), 143.* https://doi.org/10.3390/jmse6040143

[3] Camus, P., Tomás, A., Díaz-Hernández, G., Rodríguez, B., Izaguirre, C., Losada, I.J. (2019). Probabilistic assessment of port operation downtimes under climate change. *Coastal Engineering 147*, 12-24. https://doi.org/10.1016/j.coastaleng.2019.01.007

[4] Bae, H.U., Yun, K.M., Yoon, J.Y., Lim, N.H., 2016. Human Stability with respect to overtopping flow on the breakwater, *International Journal of Applied Engineering Research*, vol. 11, No. 1, 111-119.

[5] Sandoval, C., Bruce, T., 2017. Wave overtopping hazard to pedestrians: video evidence from real accidents, *Proc. of Coasts, Marine Structures and Breakwaters 2017. Realising the Potential*. 5 - 7 September 2017 - Liverpool Waterfront, UK. Paper 146. pp. 501-512.

[6] Endoh, K., Takahashi, S., 1995. Numerically modelling personnel danger on a promenade breakwater due to overtopping waves, *Proc. 24th International Conference on Coastal Engineering*, ASCE, 1016-1029.

[7] Jonkman, S.N., Penning-Rowsell, E., 2008. Human stability in flood flows, *Journal of American Water Resources Association (JAWRA)* 44(5), 1208-1218. https://doi.org/10.1111/j.1752-1688.2008.00217.x

[8] Karvonen, R.A., Hepojoki, A., Huhta, H.K., Louhio, A., 2000. The use of physical models in Dam-break analysis. *RESCDAM final report. Helsinki University of Technology*, Finland.

[9] Abt, S.R., Wittler, R.J., Taylor, A., Love, D.J., 1989. Human stability in a high flood hazard zone, *Water Resources Bulletin 25*, 4, 881-890.

[10] Mares-Nasarre, P., Molines, J., Gómez-Martín, M.E., Medina, J.R., 2018. Analysis of the overtopping layer thickness on low-crested mound breakwaters, *Coastlab18, Proc. of 7th CoastLab international conference,* 22-26th May 2018, Santander, Spain (in press).

[11] Van Gent, M., 2001. Wave runup on dikes with shallow foreshores, *Journal of Waterway, Port, Coastal and Ocean Engineering*, ASCE, vol. 127, No. 5, 254-262. https://doi.org/10.1061/(ASCE)0733-950X(2001)127:5(254)

[12] Van Gent, M., 2002. Wave overtopping events at dikes, *Proc. 28th International Conference on Coastal Engineering*, World Scientific, 2203 - 2215. https://doi.org/10.1142/9789812791306_0185

[13] Schüttrumpf, H., Möller, J., Oumeraci, H., 2002. Overtopping flow parameters on the inner slope of seadikes, *Proc. 28th International Conference on Coastal Engineering*, World Scientific, 2116-2127. https://doi.org/10.1142/9789812791306_0178

[14] Schüttrumpf, H., van Gent, M., 2003. Wave overtopping at seadikes, *Proc. Coastal Structures 2003*, ASCE, 431-443.

[15] Bosman, G., Van der Meer, J.W., Hoffmans, G., Schüttrumpf, H., Verhagen, H.J., 2009. Individual overtopping events at dikes, *Proc. 31st International Conference on Coastal Engineering*, World Scientific, 2944-2956. https://doi.org/10.1142/9789814277426_0244

[16] Van der Meer, J. W., Hardeman, B., Steendam, G., Schïuttrumpf, H., Verheij, H., 2010. Flow depths and velocities at crest and landward slope of a dike, in theory and with the wave overtopping simulator, *Coastal Engineering Proceedings, [S.I.], n. 32, p. structures.10, jan. 2011*. https://doi.org/10.9753/icce.v32.structures.10

[17] Lorke, S., Scheres, B., Schüttrumpf, H., Bornschein, A., Pohl, R., 2012. Physical model tests on wave overtopping and flow processes on dike crests influenced by wave-current interaction, *Coastal*

Engineering Proceedings, [S.I.], n.33, p. waves.34, oct. 2012. https://doi.org/10.9753/icce.v33.waves.34

[18] Hughes, S.A., Thornton, C., Van der Meer, J., Scholl, B., 2012. Improvements in describing wave overtopping processes*, Coastal Engineering Proceedings, [S.I.], n.33, p. waves.35, oct. 2012.* https://doi.org/10.9753/icce.v33.waves.35.

[19] Hughes, S.A., Nadal, N.C., 2009. Laboratory study of combined wave overtopping and storm surge overflow of a levee, *Coastal Engineering 56*, 543-558. https://doi.org/10.1016/j.coastaleng.2008.09.005

[20] Mansard, R.P.D. and Funke, E.R. (1980). The measurement of incident and reflected spectra using a least squares method. *Proc. 17th International Conference on Coastal Engineering*, ASCE, 140(1), 100-108.

[21] Herrera, M.P., Medina, J.R., 2015. Toe berm design for very shallow waters*, Coastal Engineering 103,* 67-77. https://doi.org/10.1016/j.coastaleng.2015.06.005

[22] Gómez-Martín, M.E., Medina, J.R., 2006. Damage progression on cube armored breakwaters, *Proc. 30th International Conference on Coastal Engineering,* World Scientific, 5229-5240.

[23] Gómez-Martín, M.E., Medina, J.R., 2014. Heterogeneous packing and hydraulic stability of cube and Cubipod armor units, *Journal of Waterway, Port, Coastal and Ocean Engineering 140(1)*, 100-108. https://doi.org/10.1061/(ASCE)WW.1943-5460.0000223

[24] Figueres, M., Medina, J.R., 2004. Estimating incident and reflected waves using a fully nonlinear wave model, *Proc. 29th International Conference on Coastal Engineering*, World Scientific, 594-603. https://doi.org/10.1142/9789812701916-0047

[25] Battjes, J.A. and Groenendijk, H.W., 2000. Wave height distributions on shallow foreshores, *Coastal Engineering 40*, 161-182. https://doi.org/10.1016/S0378-3839(00)00007-7

[26] Verhagen, H.J., Van Vledder, G., Eslami Arab, S., 2008. A practical method for design of coastal structures in shallow water, *Proc. 31st International Conference on Coastal Engineering*, World Scientific, Vol. 4, 2912-2922. https://doi.org/10.1142/9789814277426_0241

[27] Molines, J., Medina, J.R., 2015. Calibration of overtopping roughness factors for concrete armour units in non-breaking conditions using the CLASH database. *Coastal Engineering 96,* 62-70. https://doi.org/ 10.1016/j.coastaleng.2014.11.008

[28] Conover, W.J., Practical nonparametric statistics, John Wiley & Sons Inc., New York, 1971.